APPLIED PHYSICS REVIEWS

Plasma under control: Advanced solutions and perspectives for plasma flux management in material treatment and nanosynthesis

O. Baranov,[1] K. Bazaka,[2] H. Kersten,[3] M. Keidar,[4] U. Cvelbar,[5] S. Xu,[6] and I. Levchenko[6,2]
[1]*National Aerospace University "KhAI," Kharkov, Ukraine*
[2]*School of Chemistry, Physics, and Mechanical Engineering, Queensland University of Technology, Brisbane, Queensland 4000, Australia*
[3]*Institute of Experimental and Applied Physics, University Kiel, D-24098 Kiel, Germany*
[4]*The George Washington University, Washington, DC 20052, USA*
[5]*Jozef Stefan Institute, Ljubljana, Slovenia*
[6]*Plasma Sources and Applications Centre, NIE, Nanyang Technological University, Singapore*

(Received 26 May 2017; accepted 21 August 2017; published online 3 November 2017)

Given the vast number of strategies used to control the behavior of laboratory and industrially relevant plasmas for material processing and other state-of-the-art applications, a potential user may find themselves overwhelmed with the diversity of physical configurations used to generate and control plasmas. Apparently, a need for clearly defined, physics-based classification of the presently available spectrum of plasma technologies is pressing, and the critically summary of the individual advantages, unique benefits, and challenges against key application criteria is a vital prerequisite for the further progress. To facilitate selection of the technological solutions that provide the best match to the needs of the end user, this work systematically explores plasma setups, focusing on the most significant family of the processes—control of plasma fluxes—which determine the distribution and delivery of mass and energy to the surfaces of materials being processed and synthesized. A novel classification based on the incorporation of substrates into plasma-generating circuitry is also proposed and illustrated by its application to a wide variety of plasma reactors, where the effect of substrate incorporation on the plasma fluxes is emphasized. With the key process and material parameters, such as growth and modification rates, phase transitions, crystallinity, density of lattice defects, and others being linked to plasma and energy fluxes, this review offers direction to physicists, engineers, and materials scientists engaged in the design and development of instrumentation for plasma processing and diagnostics, where the selection of the correct tools is critical for the advancement of emerging and high-performance applications. *Published by AIP Publishing.* https://doi.org/10.1063/1.5007869

TABLE OF CONTENTS

I. INTRODUCTION 2
II. PLASMA UNDER CONTROL: BASIC CONFIGURATIONS AND SOLUTIONS 4
A. General aspects of plasma generation 4
B. Electrostatic control 5
1. Electrostatic confinement 5
2. Ion implantation 6
3. Plasma immersion ion implantation and deposition 6
C. Electromagnetic control 8
1. Incorporated substrate scheme 8
a. Closed drift configuration at the plasma generation region 9
b. Magnetically enhanced RF discharges. 12
c. RF control of ion flux in CCP discharges 13
2. External substrate scheme 14
a. Array of ferromagnetic enhanced inductive plasma sources 14
b. Array of helicon plasma sources 15
c. External substrate scheme: Neutral loop configuration at the plasma generation region 15
d. Set of magnetic mirrors along the chamber walls 16
e. Multi-slot antenna and external magnetic field to control microwave plasma 17
f. Open drift configuration: Magnetic mirror at the plasma generation region 18
g. Systems incorporating two magnetic mirrors with perpendicular axes 19
h. Magnetic mirror under substrate in line with magnetic mirror at the plasma generation region: Coaxial arrangement of electromagnets 20
i. Systems incorporating two complex magnetic mirrors with parallel axes ... 21

III. PRACTICAL EXAMPLES: APPLICATION FOR MICRO- AND NANOSYNTHESIS 25
IV. PERSPECTIVES AND TRENDS 28
A. Make it simple 30
B. Make it sophisticated 30
C. Make it large 30
D. Make it small 31
V. CONCLUDING REMARKS 31

I. INTRODUCTION

A wide range of material treatment and nanosynthesis technologies can be significantly enhanced by the use of a plasma-based process environment, with the benefits ranging from drastically increased treatment rate to improved, sophisticated control over the formation of complex, hierarchical structures and metamaterials due to the precise delivery of material and energy fluxes to the target surface.[1,2]

As most technological plasmas are generated in the close vicinity or direct contact with the target surface, the likelihood of contamination of processed material is minimal, enabling the use of these technologies in areas where the quality of the surfaces is critical for their application and performance.[3] As a result, the breadth of plasma-enhanced technologies spans surface modification,[4] chemical functionalization,[5] physical structuring, and deposition of high-quality uniform films[6] as well as very complex, multi-tier nanostructures,[7] nanodot arrays,[8] and graphenes.[9,10] The areas where these technologies can deliver benefits are equally diverse, from enhancing the optical and mechanical properties of reflective coatings[11,12] and magnetic films[13] to improving durability and wear resistance of mechanical components[14,15] and tuning the biological activity of biomaterials.[16,17] Several typical examples of plasma-based reactors and plasma sources are depicted in Fig. 1.

✓Over the last several decades, there has been a paradigm shift towards technologies that not only can deliver high-quality materials and structures but also do in a way that minimizes the use of input materials and energy consumption.

In practical terms, this meant reducing the duration and staging of the process, e.g., favoring single-step, single-environment synthesis at lower temperature and where practical,

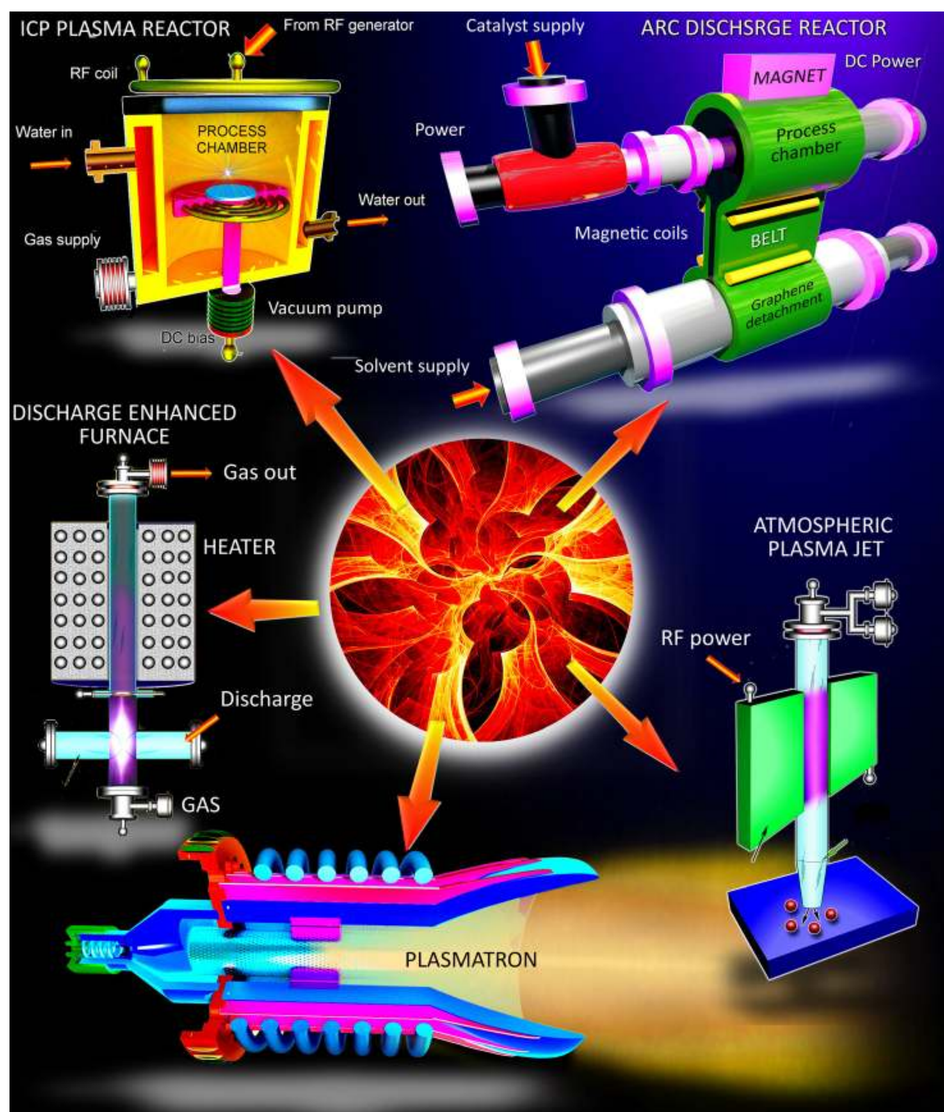

FIG. 1. Several typical examples of plasma reactors featuring different mechanisms of ignition, sustaining, and control of technological low-temperature plasmas. Inductively coupled plasma (ICP) reactor sustains the plasma inside the reactor chamber by the action of electromagnetic induction, whereas the reactor incorporating vacuum arc and magnetron plasma sources sustains the plasma mainly due to strong direct currents. The discharge-enhanced process furnace combines high (above 1000 °C) reactive gas temperature with the glow discharge plasma. Atmospheric plasma jet is sustained by the radio frequency electromagnetic fields, and DC plasmatron generates dense highly ionized plasma by the interaction of DC current with an external magnetic field.

at atmospheric pressure. Processes that can be easily integrated into existing production workflow, e.g., roll-to-roll assembly of large-area optoelectronic devices, are particularly preferred.[18,19] In general, plasma-enabled surface processing has the potential to meet these efficiency criteria,[20] with the capacity to deliver single-step treatment of large surface areas on a wide range of substrates in a highly controllable manner. The ability to control the mass flows minimizes loss of material to the environment and waste generation, thus enabling molecule- and atom-efficiency;[21,22] whereas the ability to localize the chemical and thermal activity to the surface of the substrate enables energy efficiency. Furthermore, high chemical reactivity of plasma environment increases the rate of reactions and enables *in situ* functionalization, substantially reducing the overall processing time.

Strong empirical evidence suggests that in order to effectively control physico-chemical characteristics of the materials and structures synthesized by plasma, *it is critical to control the magnitude and direction of the mass and energy flows within the processing environment, i.e., mainly the ion and electron fluxes.* Independent control over ion energy and density of ion current to the surface of the target processed structure is particularly significant in governing the outcomes of plasma processing.[23] For instance, an increase in ion energy from 30 to 500 eV during the sputtering deposition of boron-modified polysilazane led to a change in the hardness of these films in a range of 30 to 45 GPa.[24] Similarly, variation in the ion current density from 1.8 to 8.0 mA/cm^2 during the ion-assisted deposition of amorphous SiO_2 structures resulted in hardness increase from 1.0 GPa to 6.0 GPa.[25] Even more significant differences were reported in resistivity of TiN films synthesized by low-energy ion beam-assisted deposition[26] (Fig. 2), where changes in ion energy and temperature from 50 to 300 eV and from 25 to 300 °C, respectively, resulted in 10-fold change in resistivity.[27] These examples are numerous[28] and often hard to systematize due to differences in plasma setups, processing parameters, and precursor materials; yet *all suggest the significance of ion flux and energy as a primary processing control*.[29]

The ion-to-neutral flux ratio is another effective knob to control the properties of plasma-synthesized structures and nanomaterials. For instance, magnetron-deposited TaN showed a 20% increase in atomic density and 3 GPa change in residual stress when the ion-to-neutral ratio J_i/J_{Ta} was increased by the order of magnitude.[30] Similarly, an increase in the ion current to the surface due to a direct contact with plasma resulted in efficient catalyst-free growth of carbon nanotubes on silicon.[31] The changes in the fundamental properties of plasma-synthesized structures as a function of processing parameters have also been reported for many other materials and techniques. For instance, magnetron sputtered ZrC material demonstrated a 4-fold increase in resistivity and more than 4-fold change in grain size in response to changes in deposition temperature from 25 °C to 290 °C.[32] Carbon and silicon films produced by magnetron sputtering[33] and ICP plasmas showed a change in optical band gap from 1.9 to 1.3 eV in response to the increase in the

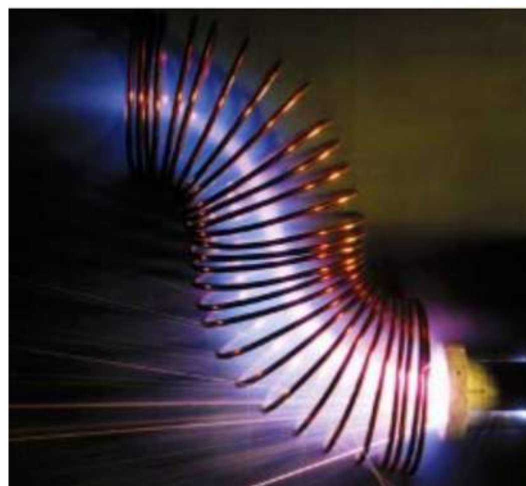

FIG. 2. An example of plasma guidance and particle separation by the static magnetic field. Open-shutter photograph showing the separation of macroparticles and cathodic arc plasma in an open S-filter. Graphite cathode, vacuum base pressure 10 torr, arc current, and coil current in series, both 1 kA for 500-μs arc pulse duration. The filter coil consists of two 90°-curved filter segments. Solid particles move linearly (bright lines on the photo) and leave the system, whereas plasma is efficiently deflected along the duct and supplied particle-free to the exit (top of the photo). Reprinted with permission from A. Anders, IEEE Trans. Plasma Sci. **30**, 108 (2002). Copyright 2002 IEEE.

substrate temperature from 100 to 500 °C.[34] Similar effect was observed when amorphous carbons were fabricated using filtered cathodic vacuum arc deposition,[35] suggesting the significance of this control across different setups and different types of nanomaterials. In addition to the properties of the deposited structures, the strength of adhesion to substrate can be controlled by tuning the ion current density. For instance, a variation in power of radio frequency ICP reactor from 0 to 60 W resulted in a rise of Ti–Al–N nanocrystal hardness from 29 to 31 GPa, with a maximum of 34.7 GPa and minimum friction coefficient of 0.13 obtained at 50 W.[36]

> ✓*These are just few examples that highlight the importance of processing parameters such as ion fluxes and deposition temperature for controlling the properties of the resultant structures and nanomaterials.*

Significant efforts have also been made to understand the mechanisms that govern the assembly of nanomaterials and nanostructures under different ion energy and current density conditions. It is quite apparent that the heat flux, and thus the temperature of the substrate, are directly affected by the energy and density of ion current from the plasma; in turn, the substrate temperature has a profound effect on the mechanism of nucleation and growth of surface-bound structures.[37,38] Others have suggested the ion energy to be a more accurate parameter in place of gas pressure,[39] and the mobility of individual grain boundaries within the film to be the critical parameter that defines the grain structure.[40,41] It has been finally demonstrated that surface modification based on ion flux may be best described by an *extended structure zone diagram*, where a generalized temperature parameter represents a sum of a homologous temperature and a temperature

FIG. 3. Typical process workflow for the assembly of nanostructured surface architectures. Starting from surface cleaning or removal of upper damaged layers, several sub-layers are formed by deposition and further, the targeted structured material is formed upon functionalization of the deposited layers.

shift arising from the potential energy of particles bombarding the surface, whereas a normalized energy represents the displacement and thermal effects arising from the kinetic energy of particles delivered to the surface.[42]

> ✓*For efficient control on the plasma-based nanomaterial synthesis, it is important to differentiate the individual effects that arise from ion energy, ion current density, and other factors.*

This can be demonstrated on the example of TiN and TaN nanostructures, where ion energy and the related ballistic effects are not the key determinants of the resultant structure.[30,43] Indeed, it is the *concomitant growth of structures with different degree of crystallinity* and associated flux of reactive species from the plasma to the substrate that govern the major properties of the film.

The uniformity of the ion current density to substrates also plays a significant role, as demonstrated in the synthesis of copper oxide nanowires[44] and vacuum arc deposited TiN films.[45] In the latter example, process yield is affected by the porosity, which reduces the effective operating area of the substrate, and the associated reduction in the ion current density to $< 30–35\ \mathrm{A/m^2}$. On the other hand, intense ion flux may lead to erosion and sputtering of the materials in contact with plasma, leading to plasma contamination and associated plasma instabilities.

It is therefore essential that the ion current and energy densities are considered as important process parameters that govern the non-equilibrium chemistry in gas phase and the assembly of surface-bound structures and an important control for large-scale, high-throughput plasma processing. We will thus distinguish the key stages of plasma-enhanced synthesis (Fig. 3) and how these stages are constrained by different configurations used to control the movement of plasma species within the processing environment.

Apparently, the manner by which a substrate interacts with a plasma-generating circuit plays an important role in the progress of these stages. Among all range of schematic solutions, we will distinguish the two main architectures, as shown in Fig. 4.

Both configurations are widely used in industry and should abide by the efficiency requirements, i.e., the effective delivery of ion and energy fluxes to the substrate and shaping the distribution of these fluxes over the substrate.

This review tries to systematize a wide diversity of existing schematic solutions in the design and development of the instrumentation for plasma processing and offers a guide to physicists, engineers, and materials scientists working in the field of plasma-enabled material processing where the selection of the correct tools is critical for the advancement of emerging and high-performance applications.

II. PLASMA UNDER CONTROL: BASIC CONFIGURATIONS AND SOLUTIONS

A. General aspects of plasma generation

Plasma is a quasineutral medium of charged particles, where densities of positive and negative charges are approximately equal, and the size of the domain occupied by the plasma greatly exceeds the Debye length.[3] Plasmas can be described as electropositive, where a removal of an electron from a neutral atom results in the formation of predominantly positively charged ions, or electronegative plasmas,

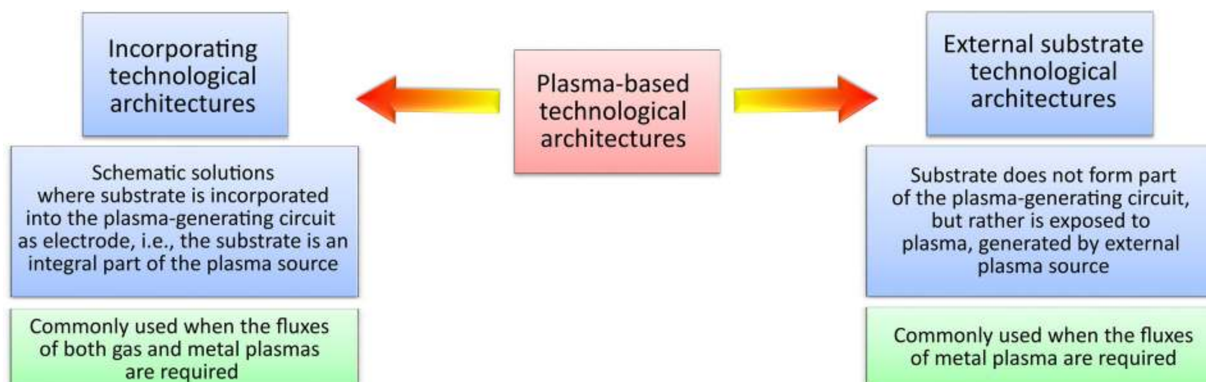

FIG. 4. Plasma-based technological architectures. The two large sub-groups of the whole spectrum of plasma-based technological architectures could be introduced, namely, "incorporating architectures" and "external architectures."

where in addition to positively charged ions, a significant number of negatively charged ions is also present. To remove an electron, additional energy should be supplied to the neutral atom as (1) thermal energy, by heating gas atoms to temperatures of a few electron-volts; (2) by use of photons with the energy related to the OUV radiation; (3) through the long-lived excited states, where the energy of one species in the gas mixture is less than the excitation energy of the other species; and (4) electron impact ionization, which is the main pathway for the generation of plasmas in technological setups.[46] Electropositive gas plasmas are commonly used for substrate processing, e.g., plasma cleaning, activation, ion implantation, and thermal diffusion-assisted ion implantation; and electronegative discharges are employed for sputter deposition of thin films and plasma etching.

Depending on the process conditions and the nature of the plasma source, various types of plasma discharges can be produced, with glow, arc, radiofrequency, and microwave discharges most commonly used for plasma processing.[47] A glow discharge occurs when a voltage applied between two electrodes, a cathode and an anode, mounted in a vessel filled with a low-pressure gas reaches a certain value, i.e., a breakdown voltage.[48] At that point, the gas in the vessel becomes ionized, and the density of the charged particles in the discharge gap increases. A negatively charged space sheath forms near the cathode to accelerate the secondary electrons, which are produced as a result of ion bombardment of the cathode, and the glow discharge plasma becomes self-sustained once secondary electron emission occurs.[49] With the simplest design of the processing reactor, typical parameters of ion current density up to 0.1 A/m^2, discharge voltage of 1–5 kV, and the background gas pressure of about 10–1000 Pa, the glow discharge was the first plasma-enabled processing tool,[46] where sputtering of the cathode material as a result of ion bombardment could be used for surface cleaning and heating as well as for deposition of the sputtered material as a coating on other surfaces.

However, relatively high gas pressures result in the decrease in the effectiveness with which the sputtered species are transported from the cathode, as well as in contamination of the processed surfaces, whereas the low density of the discharge current limits the deposition or sputtering rate. To enable commercial utility of such discharges, a hollow cathode and a magnetron discharge concepts were developed.[50,51] In essence, these techniques aim to lengthen the run of the secondary electrons on their path from the cathode to the anode, which results in increased ionization and more effective utilization of the energy gained in the cathode sheath. In the hollow cathode discharge, the increase in the electron path is provided by the shaping of the cathode and the use of a cylinder-shaped cathode structure, where the secondary electron is trapped within the discharge by the confining space potential. In magnetron discharge, the arced magnetic field (0.005–0.03 T) is applied above the cathode surface to trap the electrons by means of Lorentz force. In both cases, the density of the ion current can exceed the value of 1000 A/m^2. Yet, at these current densities, the cathode overheating problem arises. To avoid overheating and maintain efficacy, the pulsed voltage with controlled duty cycle is applied to the cathode, as in high power impulse magnetrons.[52–54]

To produce dense highly ionized plasma (up to 100% degree of ionization, density of 10^{17}–10^{18} m^{-3}) of metals and electrically conductive materials, vacuum arc discharge plasma sources were developed. These plasmas exploit the tendency of abnormal glow discharges to transition through instable glow-arc transition region into arc discharges.[55,56]

To avoid the requirement for high pressure environment in the processing chamber, the radio-frequency discharges, such as capacitively and inductively coupled discharges, were developed. These discharges operate in a frequency range of 1–100 MHz, typically at 13.56 MHz, and a pressure range of 0.1–10^3 Pa.[57,58] In capacitively coupled plasmas, the discharge is sustained by RF power applied to an electrode immersed in the plasma and can be enhanced by the use of magnetic field above the electrode surface.[59] However, the presence of the biased electrode may result in plasma contamination, a limitation that can be addressed by the electrodeless inductively coupled discharges.[60,61] Magnetic field is also applied in the RF discharges to expand the plasma density range of about 10^{15}–10^{19} m^{-3} in the helicon plasma.[62,63] The introduction of the constant magnetic field of a certain value proved to be useful not only in radio frequency but also in microwave frequency ranges, where it can be successfully implemented in electron cyclotron resonance discharges operated usually at 2.25 GHz and 0.0875 T.[64]

To control the current density and energy of ions extracted from plasma to a substrate, various solutions are proposed. However, all of them are based on either of the two methods, i.e., the *electrostatic* and *electromagnetic* control.

B. Electrostatic control

Electrostatic fields of various configurations are applied to control the ion energy and flux to a processed substrate, and ion extraction from plasma is used for the purpose. In ion implantation technique, ions are extracted far from the substrate, necessitating their subsequent transport and steering towards the substrate as an ion beam. On the other hand, in plasma immersion ion implantation and deposition (PIII&D), the ions are extracted in the close vicinity of the substrate.

1. Electrostatic confinement

To overcome the lack of control of the ion density over the large substrate, various schemes of electrostatic confinement have been developed, which are the modifications of the PIII&D technique. By applying electrostatic plasma sheath to reflect plasma electrons repeatedly from a negatively biased substrate as they traverse from the electric circuit cathode to the anode, it is possible to greatly increase the likelihood background gas ionization. For example, a plasma immersion ion implantation setup where electrostatic confinement of electrons is enabled by a hollow cathode discharge has been shown to have a significantly increased

plasma flux extracted from the glow discharge to the substrate [Fig. 5(c)].[65]

One of the typical systems implementing this type of control was based on a conventional CVD reactor, which has been enhanced by elongating the glass cylinder to extend further out from the furnace. The gained extra length of the tube allowed for the fitting of three electrodes, i.e., two cathodes and an anode, for plasma generation, and addition of glass appendages with flanges through which housed ancillary electrodes and probes for plasma diagnostics. Thus-modified CVD system is highly flexible, since the plasma glow can be selectively produced in close proximity to or further away from the high-temperature zone within the furnace, enabling plasma treatment of surfaces and plasma-assisted thermal synthesis of nanostructures, respectively.

The schematic representations of these two discharge configurations are illustrated in Figs. 6(a) and 6(b), with the photos in Figs. 6(c), 6(d), and 6(f) demonstrating the position of plasma discharges generated within these configurations.[58]

2. Ion implantation

Ion implantation is the first example of a process where electrostatic control is used to direct ion fluxes for manufacturing purposes. Conventional ion implantation is a process where ions are extracted from a plasma source (where appropriate ion species are generated) and directed to the ion beam accelerator to provide the ions with energy. To control which area of the substrate is treated, the horizontal and vertical scanning electrodes are used to deflect the ion beam electrostatically [Fig. 5(a)]. The ion implantation allows for the control of the ion energy across a wide range, i.e., $10-500$ keV, with magnetic separation of unwanted ions.[66] Yet, the control of ion current flux over a surface with complex geometry requires a mechanical manipulator, which may considerably increase the production cost and decrease the flexibility of the processing. Furthermore, high ion energy may lead to the damage of the target material structure, which may not be salvageable by means of annealing.[3] Ion implantation is widely recognized to perform profiles that peak at points inside the wafer with precise control of the dose and independent control of impurity depth and dose. Presently, various approaches have been developed to widen the range of substrates which can be treated by ion implantation that deliver considerable economic and technological benefits.[67]

However, since the most sources for ion implantation are gridded sources, they have a fundamental limitation for the ion current extracted from plasma, which is described by the Child equation:[1]

$$j_i = \frac{4}{9}\varepsilon_0\left(\frac{2eZ}{M_i}\right)^{1/2}\frac{U^{3/2}}{d^2}, \tag{1}$$

where ε_0 is the permittivity of free space, M_i is ion mass, Z is the charge state number; e is the elementary charge, U is the extraction voltage, and d is the distance between extraction electrodes.

3. Plasma immersion ion implantation and deposition

In contrast to plasma implantation, plasma immersion ion implantation and deposition (PIII&D) is able to overcome the line-of-sight limitation of the former. This is achieved by controlling the ion energy independently from the ion current density in a case of external plasma source application. This approach does not require complex and expensive systems of the ion beam extraction and steering since the treated substrate is immersed into the plasma and pulse-biased biased to a high negative potential. A relatively low constant negative bias is also applied for the deposition purposes [Fig. 5(b)].[3] A transition from the pulse to constant bias allows controlling the scale of a surface feature that can be treated uniformly through the transition from a matrix to Child law sheath with a thicknesses of 50 to 500 μm, respectively.[1] At the same time, the sheath range limits the ability of the PIII&D technique to control the distribution of the ion current over the large-scale substrates, since it determines a range of penetration of the control electric field into the plasma. The limited ability to control the ion energy and ion density distributions is an intrinsic disadvantage of the

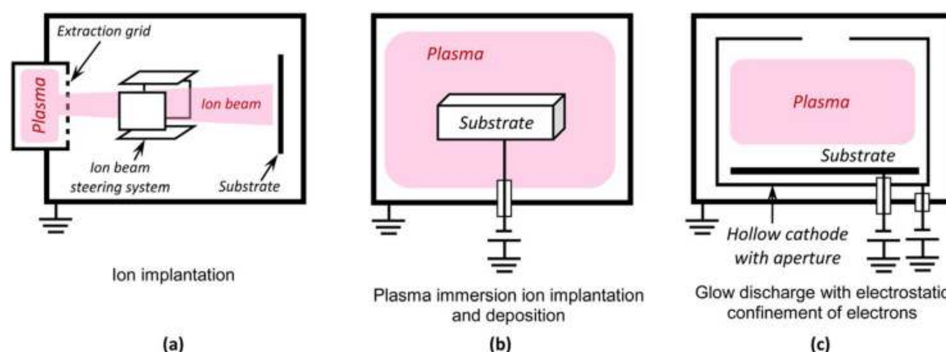

FIG. 5. Schemes of electrostatic control of ion fluxes: conventional ion implantation where ions extracted from a plasma source are accelerated by the ion beam accelerator and driven towards the substrate, with the delivery to the processing area controlled by horizontal and vertical scanning electrodes (a); plasma immersion ion implantation overcomes the line-of-sight limitation of the ion implantation, with the ion energy controlled independently from the ion current density in a case of external plasma source application and does not require complex, expensive systems of the ion beam extraction and steering, since the treated substrate is immersed into the plasma and pulse-biased to a high negative potential; a relatively low constant negative bias is applied for the deposition purposes (b); electrostatic confinement based on a hollow cathode configuration, where electrons are reflected repeatedly from the electrostatic sheath prior to reaching the anode, thus increasing greatly the probability of ionization of background gas molecules (c).

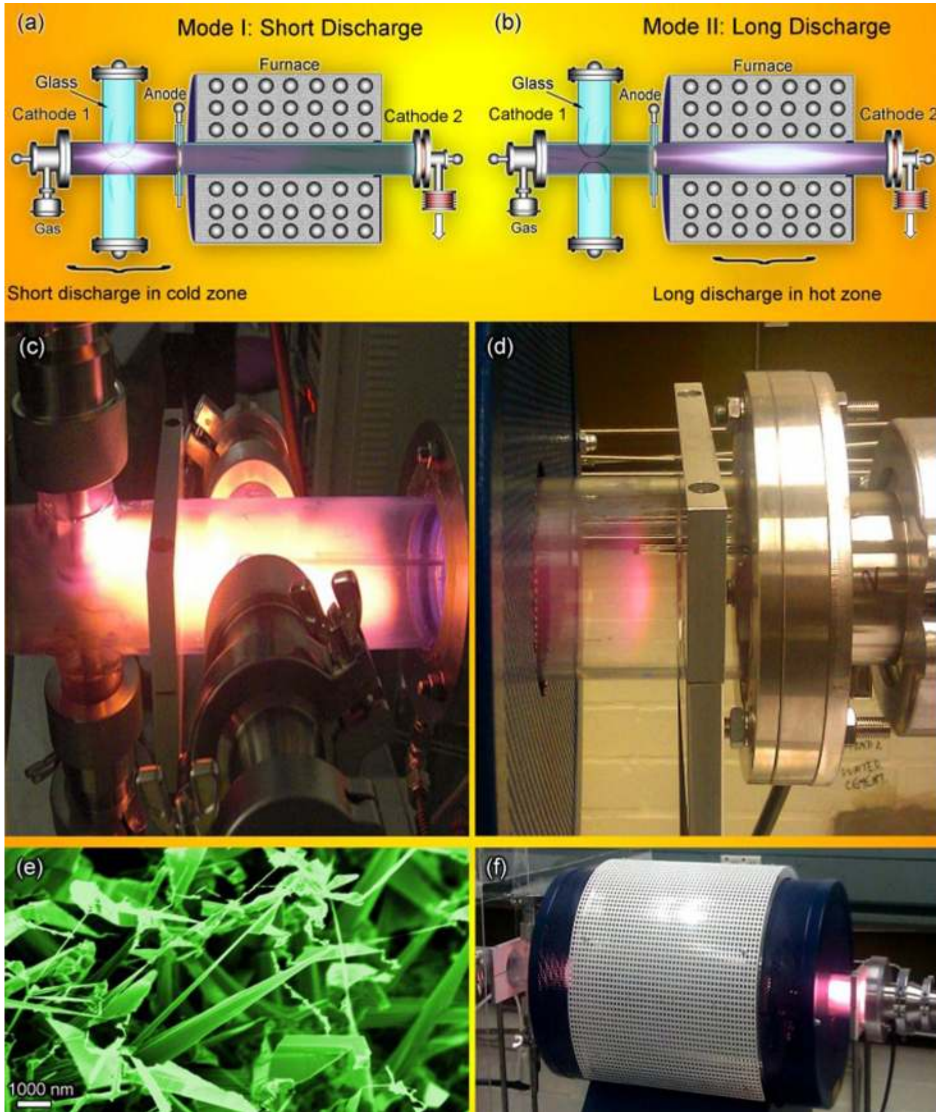

FIG. 6. Possible configurations of CVD reactor modified by the addition of a glow discharge. (a) Schematics of the short discharge in the cold zone of the modified PECVD setup. (b) Schematics of the long discharge in the hot zone of the modified PECVD setup. (c) Photo of the plasma in the short discharge. (d) Photo of the plasma in the long discharge—cathode glow separated from the positive column by the cathode dark space is clearly visible. (e) Representative scanning electron microscopy image of hierarchical ZnO nanowires produced in the modified reactor. (f) General view of the modified PECVD system with the discharge ignited in the long configuration. Reprinted with permission from Primc *et al.,* IEEE Trans. Plasma Sci. **42**, 2564 (2014). Copyright 2014 IEEE.

PIII&D technique. Yet, its application range is much wider in comparison with the conventional ion implantation due to much simpler design and wider range of substrates that can be treated in a cost-efficient way.

Unlike the interaction of a surface with neutral gas, the interaction with plasma results in generation of an electrically charged sheath between the surface and plasma. When the substrate is pulse-biased, a matrix sheath is formed at the initial stage with a thickness[1]

$$S_m = \lambda_{De}\left(\frac{2U_s}{T_e}\right)^{1/2}, \tag{2}$$

where $\lambda_{De} = (\varepsilon_0 T_e/en_s)^{1/2}$ and n_s are the electron Debye length and plasma density at the sheath edge; T_e is the electron temperature (eV); and U_s is the applied voltage.

Then, as the time goes, the matrix sheath expands thus converting into a transient sheath with the instant sheath thickness found from the equation:[3]

$$\tanh^{-1}\left(\frac{S_t}{S_c}\right) - \frac{S_t}{S_c} = \frac{u_B t}{S_c} + \tanh^{-1}\left(\frac{S_m}{S_c}\right) - \frac{S_m}{S_c}, \tag{3}$$

where $u_B = (eT_e/M_i)^{1/2}$ is the Bohm velocity and S_c is the thickness at the end of the expansion. The latter steady-state sheath is called Child law sheath and is described by the equation:

$$S_m = \frac{\sqrt{2}}{3}\lambda_{De}\left(\frac{2U_s}{T_e}\right)^{3/4}. \tag{4}$$

After the substitution, the time scale for establishing the steady sheath is found

$$t_c = \frac{\sqrt{2}}{9}\omega_{pi}^{-1}\left(\frac{2U_s}{T_e}\right)^{3/4}, \tag{5}$$

where $\omega_{pi} = \left(e^2 n_s/\varepsilon_0 M_i\right)^{1/2}$ is the ion plasma density.

After comparing the matrix and Child law sheathes, one can conclude that a transition from the pulse to constant bias allows controlling a scale of a surface feature that can be treated uniformly, since the typical matrix sheath thickness is about tens of λ_{De}, while for the Child law sheath, the thickness is about hundreds of λ_{De}. Thus, at the transition from a matrix to Child law sheath, the thicknesses changes from about 50 μm to about 1 cm for industrial plasma, respectively.

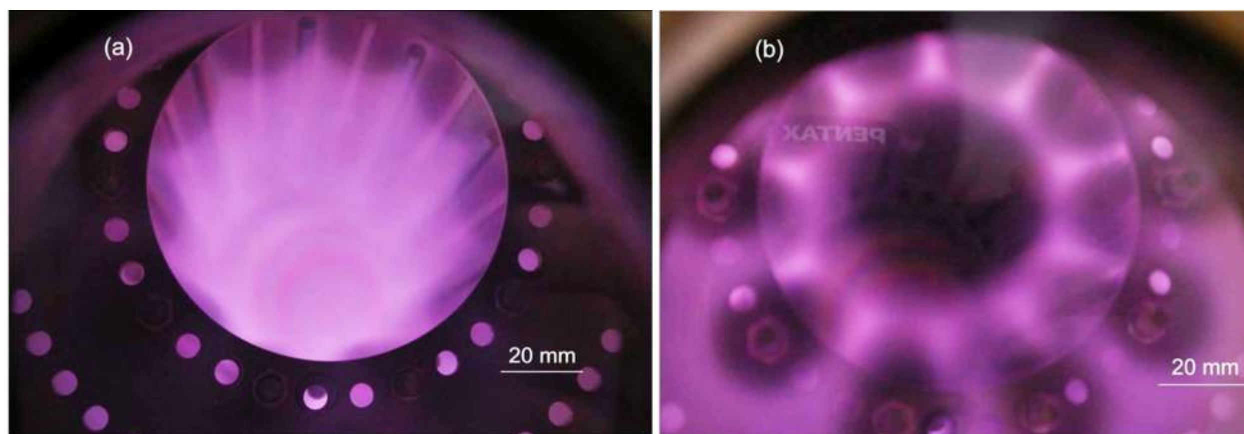

FIG. 7. (a) Electrostatic confinement under appropriate conditions. (b) Loss of confinement observed at higher gas pressures. A casing of the hollow cathode structure is designed as a set of rods; similar structure was made to be used as anode, and the cathodic and anodic rods are alternated in the assembly, thus forming a segmented hollow cathode arrangement. As supposed, the electrostatic confinement would retain a portion of the electrons within the confinement area, ultimately increasing the availability of active species in this region, and resulting in a larger current. Reprinted with permission from Gallo *et al.,* IEEE Trans. Plasma Sci. **39**, 3028 (2011). Copyright 2011 IEEE.

Figure 7 shows an example of PIII&D system for surface engineering. It relies on the modification of the hollow cathode geometry, where several sets of rods are used to make the casing of the hollow cathode.[68]The system could support processes, such as plasma nitriding and reactive deposition of sputtered material, with the loss of confinement observed at higher gas pressures. Yet, these setups do not provide for separate control of the ion current density and ion energy or the control of the ion current density distribution along the substrate surface.

C. Electromagnetic control

1. Incorporated substrate scheme

Another approach by which the direction and the shape of the distribution of the plasma fluxes can be effectively controlled in the plasma-based technological setups[69,70] and devices[71,72] relies on the use of a magnetic field,[73,74] which can selectively trap electrons but not ions at the field strength is of $\approx 20-30$ mT. The electric field that arises from the interaction of the magnetic field with the plasma flux has a spatial scale larger than that of the electrostatic sheath. This electrical field controls the movement of the plasma ions and the shape of the ion flux. With the respect to the role of the substrate in the plasma-generating circuit, two configurations are typically used to control the flux. In the incorporated substrate scheme (ISS) (Fig. 8), the substrate acts as an electrode above which the arc configuration of the magnetic field is formed. This leads to the closed electron drift that can be used to effectively control the ion fluxes. In the external substrate scheme (ESS), the plasma is generated using the external plasma source, with the substrate not being a part of the plasma-generating circuit. The magnetic traps of magnetic bottle configuration are formed.

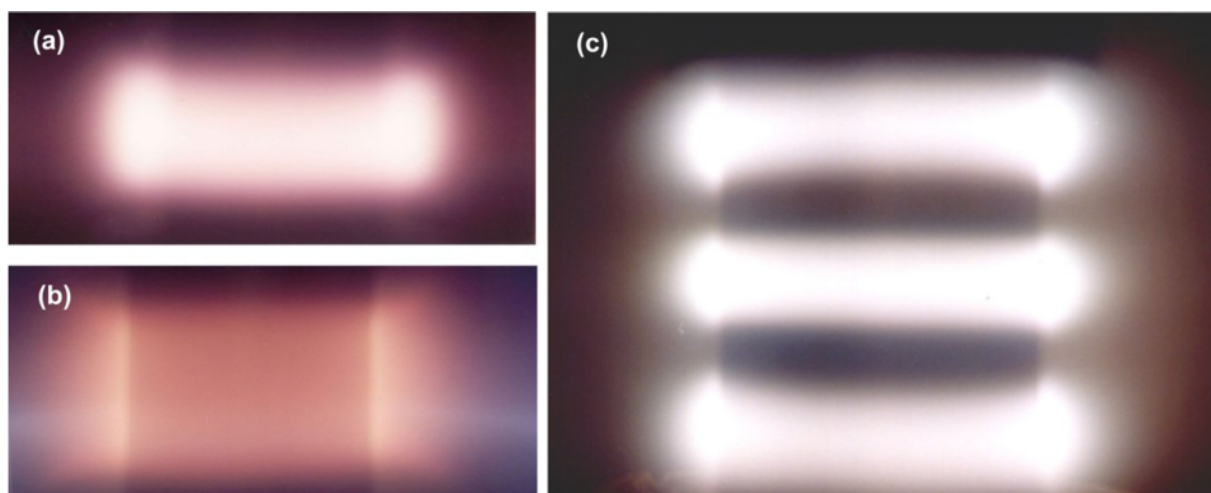

FIG. 8. Photographs of plasma discharge formed around the cylindrical substrate which houses an auxiliary set of magnetic coils: (a) low current, $U = 1600$ V; (b) high current, $U = 1000$ V; (c) several sets of coils can be powered simultaneously. The magnetron discharge evolves from a well-resolved, bright torus (a) to wider, less-resolved, cylindrical-shaped discharge (b), and to a complex plasma environment, where multi-peak distribution of the ion current density with controlled peak height for each of the peaks is produced by altering the current in each of the auxiliary magnetic coils (c). Reprinted with permission from Levchenko *et al.,* Vacuum **72**, 335 (2004). Copyright 2004 Elsevier.

a. Closed drift configuration at the plasma generation region. In this configuration, the control magnetic field is arc-shaped to lock the lines of the control magnetic field to a negatively grounded substrate and to enable a closed drift of the electrons. The discharge is generated in the proximity of the substrate by applying a bias voltage to the substrate relative to grounded walls of the deposition reactor. Upon application of the magnetic field, the plasma takes the shape of a bright torus above the substrate. This is the region of higher ionization. In the example presented in Fig. 6(a), magnetron discharge is generated around the cylindrical substrate, which also houses the coils used to produce the magnetic field. In such configuration, at a voltage of 1000 V the plasma takes the shape of a narrow, well-resolved torus, and the ion current to the substrate surface is localized. The diameter of the plasma torus is in a few cm.[75–77] In the region of the closed electron drift, the plasma is dense, with the discharge being much greater than that produced in the absence of the magnetic field. The increased power of the discharge is sufficient to bring the target area to white heat for several seconds.

Variations in the applied voltage and the magnitude of the magnetic field can be used to control the current-voltage ($I-V$) properties of the plasma, where careful optimization of the former two parameters is essential to maintain stability of the discharge. Indeed, increasing the strength of magnetic field and applied voltage beyond 0.05 T and 1000 V, respectively, has been shown to destabilize the plasma, leading to darkening of the torus and a decrease in the ion current.[75] Further increase in the value of the applied voltage results in the substantial dimming of the plasma discharge and in the disappearance of the well-resolved torus shape. As illustrated in Fig. 8(b), under these conditions, the plasma is dim enough for the surface of the underlying cylindrical substrate to be visible as a dark object. Increasing the voltage further leads to additional drop in total current, with the current values ranging from a few or tens of milliamperes subject to the pressure within the reactor, and ensuing darkening of the plasma discharge.[75] When the applied voltage controls the total current of the plasma, the arc-shaped magnetic field above the biased substrate enables the control over the nature of the ions extracted from the magnetron discharge, i.e., the energy of ions and the density of ion current. While these parameters can be controlled independently, they are linked through the current-voltage relationships. The system allows for the addition of controls over the ion current density distribution along the substrate, which can be attained by manipulating the concomitantly powered magnetic coils housed within the cylindrical body of the substrate. Under these conditions, it is possible to split the plasma discharge into a set of tori, each forming their own deposition zone, as illustrated in Fig. 8(c).[78] The density of the ion current within each deposition zone can be controlled by changing the current applied to power the corresponding coil.

The total distribution of the ion current density to the substrate can be calculated by the sum of the Gaussian distributions caused by each of the plasma ring

$$J_i(x) = \frac{1}{t_\Sigma}\sum_i^n J_{0i}\exp\left[-\left(\frac{(x-x_{0i})^2}{\Delta x_i^2}\right)\right], \quad (6)$$

where J_{0i} is the maximum of i-th distribution, x_{0i} is a location of the maximum, and Δx_i, is a width of the distribution that depends on the radius of a curvature of the arc shaped magnetic field.

The maximum J_{0i} can be determined from the ion current I_s to the substrate from the experimentally measured dependence that is described well by the approximation $I_s = aU^n$.

To facilitate large-area treatment of the surface by the ion current in the arc configuration, it is necessary to control the radius R_c of the magnetic field lines in the plasma zone. This can be achieved by using different arrangement of the magnetic core within the magnetron system. In a planar magnetron system, the possibility of such control has been demonstrated through the finite element modeling employing the magnetostatic element of FEMM™ software.[79] The possible configurations of the magnetic field over the plasma discharge are shown in Figs. 9(a), 9(d), and 9(k).[80] Images of the plasma shown in Figs. 9(b), 9(e), and 9(l) provide a visual confirmation of the control of the ion current density distribution in the systems, where the magnetic field forms an arc above the target substrate. Figures 9(c), 9(f), and 9(m) illustrate the respective ion current density distributions above the surface of the substrate, as captured by means of the planar probe.

The magnetic field configuration depicted in Fig. 9(a) is characteristic of the planar magnetron operation mode, where the cathode has a form of a disk and acts as a cathode of the magnetron source. In this configuration, the plasma discharge has a comparatively narrow width of the racetrack [Fig. 9(b)], with high plasma density in region between the inner and outer poles of the magnetron iron core in the arc-shaped magnetic trap near the substrate.[81–83] The measured distribution of the ion current density is also representative of the characteristic distribution in the planar magnetron discharge. The peak of the distribution falls within the region between the inner and outer poles of the magnetic system core [corresponding to the brightest part of the plasma discharge, see Figs. 9(b) and 9(c)].

When the cathode is changed from the disk-shaped to the hollow cathode structure by the addition of the sidewalls in the same planar magnetron system, the volume containing the magnetically confined electrons is increased owing to the presence of the side surface of the cathode [Fig. 9(d)]. The shape and brightness of the discharge are changed significantly, as illustrated in Fig. 9(e). Above the peripheral cathode surface, the brightness of the plasma is higher than that of the discharge shown in Fig. 9(b). Nevertheless, the most intense portion of the discharge remains within the region between the magnetic system poles. The distribution of the ion current is also considerably affected by the addition of the sidewalls above the magnetic system. Figure 9(f) illustrates probe measurements of this distribution, highlighting a substantial increase in the ion current in the proximity of the sidewalls.

Another planar magnetron configuration, where the hollow cathode structure without inner and outer cylindrical parts of the magnetic core is used, is shown in Fig. 9(k). In this system, the curvature radius R_c of the magnetic field lines is substantially increased in comparison with that of the aforementioned two configurations [shown in Figs. 9(a) and 9(d)]. By excluding the inner and outer parts of magnetic core and at the same time preserving the hollow-cathode structure of the substrate, it is possible to expand the plasma discharge over the entire surface of the cathode, as demonstrated in Fig. 9(l).[84–86] Corresponding probe measurements presented in Fig. 9(m) provide further confirmation of the expansion of the plasma discharge with the elimination of the magnetic core. These measurements also demonstrate a drastic change in the distribution of the ion current density, where the initial Gaussian distribution transforms into abroad plateau with a high degree of uniformity. The density of ion current to the substrate can be increased by increasing the current in the magnetic coil, without substantially affecting the shape of the distribution.

Since the application of arc configuration of the magnetic field with closed drift of electrons above the biased substrate results in the ignition of magnetron discharge,[87] the principles of magnetron operation control can be used to control the ion fluxes over the substrate when the work pieces are installed on the magnetron cathode surface, i.e., the magnetron cathode is used as the substrate.[88]

To enable the development and optimization of energy-efficient hollow-cathode magnetron discharges (Secs. II B 1 and II C 1), the key features of the dielectric breakdown within the system was explored experimentally and numerically, with the details of this study reported elsewhere.[84] The electrical breakdown can be described using:

$$U_b = \frac{B_c P d}{ln\left[A_c P d\left(1+\frac{h}{d}\left(\frac{h_m}{h}\exp\left[-\frac{B_c P d}{U_b}\left(\frac{\lambda_a}{\lambda_a^*}-1\right)\right]-1\right)\right)\right] - ln\left[ln\left(1+\frac{1}{\gamma_{net}}\right)\right]}, \tag{7}$$

where $A_c = \sigma_a/kT$ and $B_c = \varepsilon_{iz}\sigma_a/kT$; k is Boltzman constant, P and T are the gas pressure and temperature, respectively; σ_a is the cross section for electron-neutral elastic collisions; U_b is the breakdown voltage; h is the height of the hollow cathode structure; d_m is the total path the electrons have to traverse to overcome the confinement region; λ_a^* is the path length across the magnetic field where the electrons gain energy between the elastic collisions with neutrals; λ_a is the path length for elastic collisions of the electrons with neutrals; γ_{net} is the effective coefficient of the secondary electron emission in the presence of the magnetic field; and d is the distance between the cathode and the anode.

In the absence of the applied magnetic field, the equation is effectively reduced to the conventional Paschen's law, whereas when such field is finite, the numerical solution to Eq. (7) can be produced.

Another model was developed to describe the transport of plasma in the crossed magnetic and electric fields,[81] and thus provide an explanation for the obtained $I-V$ behavior of the planar magnetron discharge. As shown in Fig. 9(a), the magnetic field lines have the radius of curvature R_c. As the electrons collide with the neutral background gas molecules, their energy $\varepsilon(x)$ is lost, controlling the range L_{pr} of these electrons within the ionization gap L_{ion}. When $\varepsilon(L_{pr}) = \varepsilon_{Lion}$, electron conduction across the magnetic field is dominated by the Bohm conductivity, and an independent discharge system is established by the sheath and ionization gap. It is then possible to express the condition of the discharge self-sustainment for the entire length $L_{ion} = L_{pr} + d$ of the ionization gap

$$\frac{\gamma}{1+\gamma}\left[1+\frac{2}{L_{pr}}\frac{U_s^{1/2}-\varepsilon_{Lion}^{1/2}}{\varepsilon_c} \times\left(\int_0^{L_{pr}}\varepsilon^{1/2}\left(1+\frac{z}{R_c}\right)dz + \int_0^{L_{pr}}\left(\varepsilon^{1/2}\left(1+\frac{z}{R_c}\right) - \frac{1}{R_c+z}\left(\int_0^{z}\varepsilon^{1/2}\left(1+\frac{z}{R_c}\right)dz - \frac{L_{pr}}{2}\frac{\varepsilon_c}{U_s^{1/2}-\varepsilon_{Lion}^{1/2}}\right)\right) \times\left(\exp\left[\alpha_i(L_{pr}+d-z)\right]-1\right)dz\right)\right] = 1, \tag{8}$$

$$L_{pr} = \left(\frac{m}{2e}\right)^{1/4}\left(\frac{2U_{pr}}{\varepsilon_c n_a \sigma_i \alpha_b B}\right)^{1/2}\left(U_s^{1/2}-\varepsilon_{Lion}^{1/2}\right)^{1/2}, \quad \text{and}$$

$$\varepsilon^{1/2} = U_s^{1/2} - \frac{U_s^{1/2}-\varepsilon_{Lion}^{1/2}}{L_{pr}}z, \tag{9}$$

where U_{pr} is the potential drop on the range L_{pr}; U_s is voltage drop across the sheath; ε_c is the collision energy loss per electron-ion pair created, eV; n_a is neutral atom density, m^{-3}; σ_i is cross section for ionization electron collisions with neutrals, m^2; and α_b is a constant.

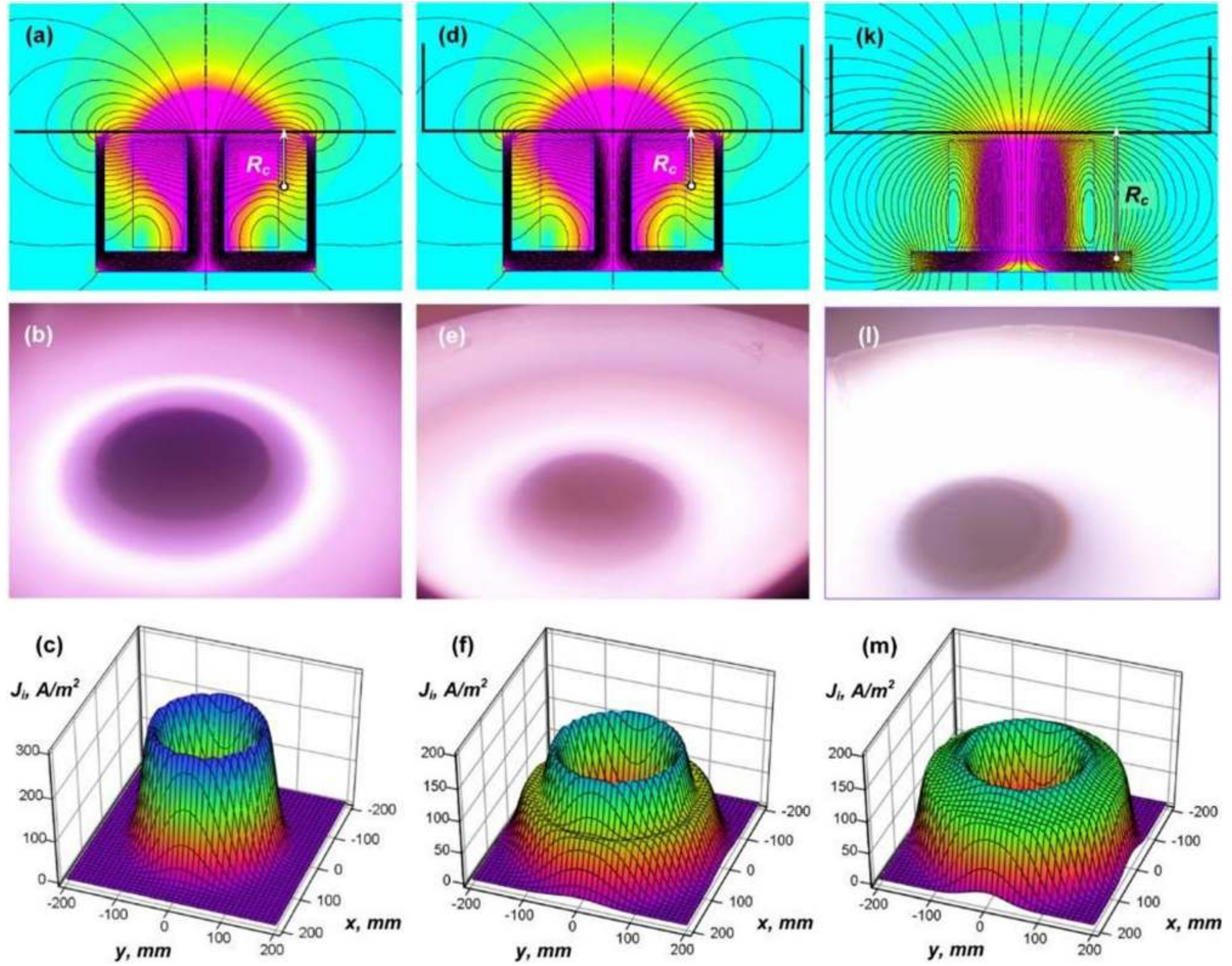

FIG. 9. Structure of the magnetic field [(a), (d), and (k)]; photographs of plasma discharges [(b), (e), and (f)], and distributions of the ion current density [(c), (f), and (m)] over the substrate surface in a setup with the arc magnetic field above the substrate and different modes of the magnetic core: (a)–(c)—planar magnetron mode; (d)–(f)—planar magnetron with a hollow-cathode structure mode; (k)–(m)—planar magnetron without parts of the core and with a hollow-cathode structure mode. The evolution of the plasma discharge and distribution of the ion current density along the substrate surface from the narrow peak (c) to the wide distribution (m) can be observed. Reprinted with permission from Baranov *et al.,* Mater. Chem. Phys. **188**, 143 (2017). Copyright 2017 Elsevier.

The expression for the $I-V$ characteristic of thus-produced plasma discharge was derived from the empirically measured and theoretically derived relationship between the magnetron discharge current and the neutral gas density.[89,90] The complex geometry of most technological setups necessitates that the simplifying assumptions are made, where the heat conduction within a spherical geometry is considered. The heat source is described in terms of its minimal radius r_t, which is derived from the values of sputter trench width w_s and internal radius R_{min}. The radius of the rarefied region is derived by adding several number f of mean free paths λ_a (to account for the collisions between the ejected atoms and that of the gas) to the radius r_t. Therefore, the density of the gas within the rarefied region can be expressed as[83]

$$n_H = 2n_0\left(1 - \frac{I\Upsilon_v E_a}{4\pi K l T_0} - \frac{\sigma n_0}{f} r_t + \sqrt{\left(1 - \frac{I\Upsilon_v E_a}{4\pi K l T_0} - \frac{\sigma n_0}{f} r_t\right)^2 + \frac{I\Upsilon_v E_a}{\pi K T_0}\frac{\sigma n_0}{f}\left(\left(\frac{4\pi K T_0}{I\Upsilon_v E_a} + \frac{1}{l}\right) r_t + 1\right)}\right)^{-1}, \quad (10)$$

where n_H is gas density in the rarefied region near the magnetron cathode, m^{-3}, and n_0 is gas density in "background" region near the chamber walls; σ is cross section for atomic collisions with neutral gas species, m^2; T_0 is temperature of the walls of the processing reactor; r_t is the radius of the hemispherical heat source; l is the distance from the heat source center (center line of sputter trench) to the chamber walls; K is thermal conductivity of the gas; I is discharge current, A; Y_v is sputter yield; and E_a is energy of sputtered atom, eV.

By substituting n_a with n_H in the expression for the condition of the discharge self-sustainment, the $I-V$ characteristics of the plasma magnetron discharge can be attained.

When operated in the stationary mode, the $I-V$ characteristics of the discharge represent the ion flux, with the distribution of the ion current along the treatment plane having Gaussian shape. The total ion current and ion energy are primarily influenced by the magnitude of the magnetic field and the pressure of the background gas.[81] In the cases when the system is operated in ISS mode, the location of the sputter trench on the surface of the magnetron cathode defines the place on which the treated objects should be positioned. The properties of the magnetic field determine the width of the sputter track as[1]

$$w_s \approx 2(2r_{ce}R_c)^{1/2}, \tag{11}$$

where r_{ce} is Larmor radius of the magnetized electron, and R_c is curvature radius of the magnetic field lines near the cathode in a region of the magnetron discharge [Fig. 9(a)].

Indeed, in the ISS system where the substrates also acts as an electrode in the plasma-generating circuit, the pressure within the processing chamber and the properties of the magnetic trap, i.e., the curvature radius of the field lines and the magnitude of the field, are the key controls for the ion fluxes and critical determinants of the efficacy of the system. Hence, re-configuration of the structure of the magnetic core [Fig. 9(k)] and the employment of additions coils can be effectively used to control the radius of the curvature of the magnetic field lines.

b. Magnetically enhanced RF discharges. Magnetically enhanced reactive ion etcher (conventional and gradient MERIE) or RF magnetron is another modification of the setup with the control magnetic field located above the treated substrate. Here, the magnetic field is typically applied in capacitive discharges to circumvent the disadvantages of high sheath voltages and consequent low density of ion flux and high energy of ions at a given power level. The magnetic field is generated with a set of coils installed around the substrate perimeter. In comparison with common capacitive discharges, generation of plasma with lower sheath voltages, higher densities, and independent control of both is possible in these setups. Nevertheless, they suffer from the lack of uniformity of the plasma over the treated substrate, which can give rise to lateral dc currents within a film growing on the substrate, thereby damaging the film structure. In a similar way, inductively coupled plasma etch system can be modified, as shown in Fig. 10.[91] It is worth to note that the latter scheme can also be categorized as an external substrate scheme.

The magnetic field B applied in MERIE results in the reduction in electron cross field mobility as the magnetic field increases and produces a decrease in the dc bias that is becoming more positive. This decrease is accompanied by a decrease in the energy and an increase in the angular spread of the ion flux to the substrate.[92]

The electron flux is described as

$$\varphi_e = en_e\mu_e E - D_e \nabla n_e, \tag{12}$$

where μ_e and D_e are the tensor mobility and diffusivity, and the tensor forms of transport coefficients, A, are derived from their isotropic values, A_0, by

$$A = \frac{A_0}{\alpha^2 + B^2} \times \begin{pmatrix} \alpha^2 + B_r^2 & \alpha B_z + B_r B_\Theta & -\alpha B_\Theta + B_r B_z \\ -\alpha B_z + B_r B_\Theta & \alpha^2 + B_\Theta^2 & \alpha B_r + B_\Theta B_z \\ -\alpha B_\Theta + B_r B_z & -\alpha B_r + B_\Theta B_z & \alpha^2 + B_z^2 \end{pmatrix}, \quad \alpha = \frac{\nu m_e}{e}, \tag{13}$$

where ν is the electron momentum transfer collision frequency.

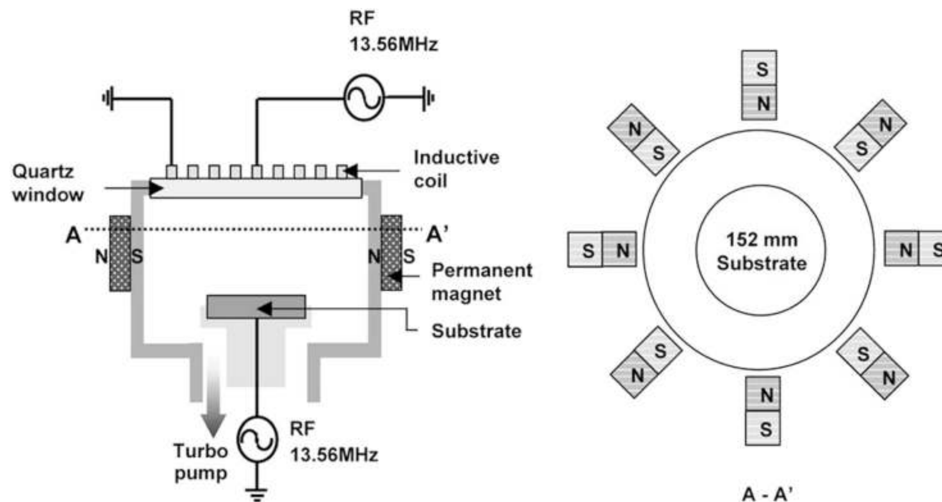

FIG. 10. Schematic diagram of the magnetically enhanced inductively coupled plasma etch system. Magnetic bucket enhances the discharge power by insulating the plasma from the chamber walls as in a case of the combined treatment by the use of capacitively coupled plasma (CCP) and inductively coupled plasma (ICP) discharge as in a case of mere CCP plasma (ISS setup), where generation of plasma with lower sheath voltages, higher densities, and independent control of both, in comparison with common capacitive discharges is possible. Reprinted with permission from Kim *et al.*, IEEE Trans. Plasma Sci. **32**, 1362 (2004). Copyright 2004 IEEE.

c. RF control of ion flux in CCP discharges. In capacitively coupled plasma (CCP) discharges, RF control of ion flux can be considered using a two-dimensional electromagnetic model originally developed by Lieberman *et al.*,[93] where the standing-wave, edge, and skin effects are regarded as chief causes of treatment non-uniformity. Standing waves are formed when the electromagnetic waves propagating outward from the radial center to the edge are superposed with counter propagating waves. The effect of the standing wave on the plasma density manifests itself as a maximum of power deposition at the discharge center, the effect becoming increasingly prominent in high frequency and large area discharges. Although electrostatic edge effects manifested as a maximum of the RF current at the discharge edges are inherent to all CCP discharges due to the small physical distance between the grounded surfaces, i.e., counter-electrode or deposition reactor walls, and the RF electrode, the contribution to field non-uniformity from electromagnetic edge effects also need to be considered. The latter arise from the sudden change in the permittivity when the wave propagating toward the radial center collides with the radial plasma edge and gives rise to transitory fields. These evanescent fields are greatest at the edge of the discharge, which, with the contribution from electrostatic edge effects, leads to large field non-uniformities with a maximum of power in the proximity of the discharge edge. At high frequencies, when plasma densities are suitably high and the skin depth is similar to the electrode gap, field non-uniformities due to skin effect become prominent. The non-uniformities arise from the large induced radial electric field concentrated at the interface between plasma sheath and bulk plasma, with its maximum, and thus the maximum of radial currents and power deposition, in the proximity of the discharge edges.

The individual contributions from these effects to the field non-uniformity and thus the treatment outcomes have been confirmed experimentally. For instance, a study of dependence of etch-rate radial distribution on driving frequency and applied RF power in the dual-frequency CCP by Sung *et al.*[94] identified standing wave and skin effects as the chief causes of plasma and thus etch-rate nonuniformities. Modification of the shape of the electrode has been shown as an effective means for minimizing the standing wave-related etch-rate nonuniformity, as shown in Fig. 11, where the replacement of the flat with the lens- or step-shaped electrode in parallel plate CCP etch reactor notably improved the uniformity of the etch-rate radial distribution. Indeed, as shown in Fig. 11(c), where the plasma setup employing flat electrode has a considerably center-to-edge etch-rate ratios, these ratios are notably smaller in the corresponding setup fitted with the stepped electrode.

Perret *et al.*[95] observed that the distribution of the ion current density in CCP discharges generated over a large area of 160 cm^2 responded to both a change in the driving frequency and that in the applied RF power, as illustrated in Fig. 12. It is evident that an increase in the driving frequency from 13.56 MHz to 81.36 MHz corresponds to a change in the shape of ion flux distribution from relatively uniform and flat to dome-shaped, which peaks at the center of the substrate [Fig. 12(a)]. On the other hand, an increase in RF power from 50 W to 265 W leads to a relative increase in the ion current along the periphery of the discharge, as illustrated in Fig. 12(b). For plasma generated at low RF power, the ion flux approaches maximum near the center of the substrate, the effect being a result of the standing-wave effect. An increase in the RF power increases electron density of the plasma, with more intense plasma emerging along the sides and in the corners of the discharge, possibly attributed to the contributions from the skin or edge electromagnetic effects.

Subsequent theoretical study of the distribution of ion energies and ion fluxes in low-pressure capacitive discharges within the same frequency range by Peret *et al.* showed that the ion energy distribution function was typically represented by a solitary peak corresponding to the time-averaged potential of the bulk of the plasma.[96] Increasing the driving frequency of the discharge was associated with the presence of lower energy ions with higher fluxes. Interestingly, unlike that for ion flux distribution, the uniformity of ion energy distribution was not affected by varying the driving frequency, even under conditions generally associated with high RF voltage distribution nonuniformity due to the presence of standing waves. This was attributed to the presence of dc current which radially flows in the plasma and electrodes.

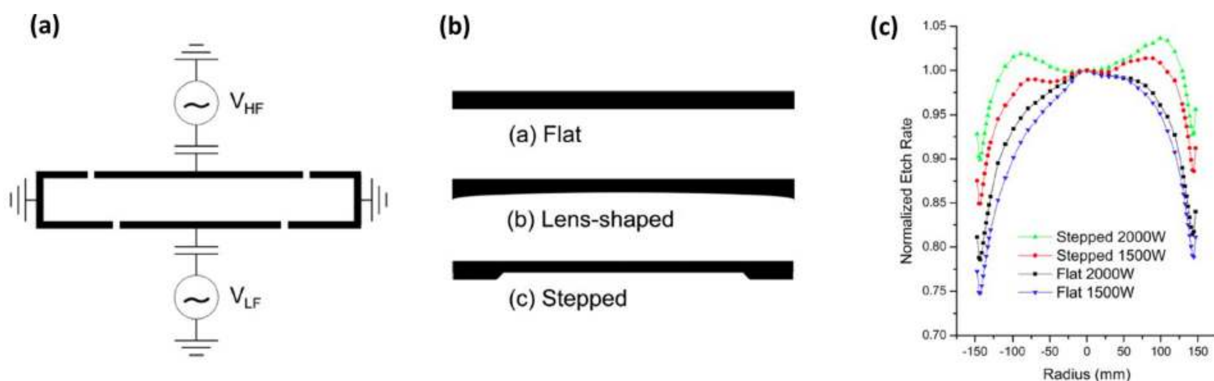

FIG. 11. (a) Schematic of a dual-frequency capacitively coupled plasma setup. (b) Possible RF electrode configurations include flat, lens-shaped, and stepped RF electrodes, shown here in the cross-sectional view. (c) SiO_2 etch rate obtained with flat and stepped top electrode (at RF frequency of 60 MHz). It is evident that the etch rate depends on the electrode shape and power used to generate the discharge, with the etch rate distribution becoming uniform for stepped electrode under higher discharge power. Reprinted with permission from Sung *et al.,* J. Vac. Sci. Technol. A **30**, 061301 (2012). Copyright 2012 AVS.

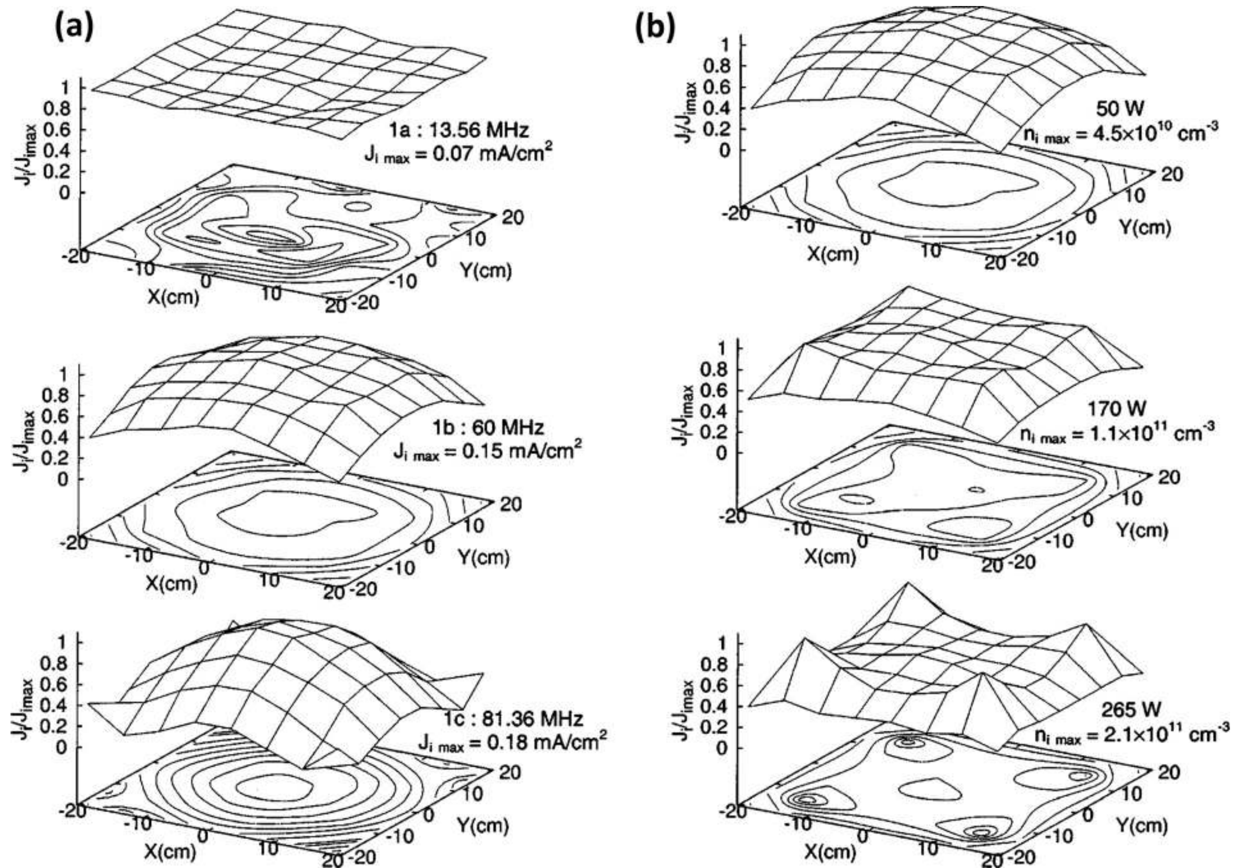

FIG. 12. Distributions of 2D ion flux as a function of driving frequency and RF power at a constant working pressure of 150 mTorr. The standing-wave effect becomes more evident as the frequency increases from 60 MHz to 81.36 MHz (a) and as the RF power increases from 50 W to 265 W at a constant frequency of 60 MHz (b). The ion current density distribution responds to an increase in the driving frequency and applied power by changing its shape from uniform to one with a central dome (a) or enhanced periphery (b), respectively. Reprinted with permission from Appl. Phys. Lett. **83**, 243 (2003). Copyright 2012 AIP Publishing LLC.

At even higher frequency of 100 MHz, Volynets *et al.*[97] showed substantial plasma nonuniformity in triode-type CCP etch reactor when it was operated in the traditional mode. The nonuniformity was attributed to the presence of electromagnetic effects, in particular, the standing wave effect and the skin effect that become prominent at low and high powers, respectively. One of the possible means to control the plasma and ensure its uniformity is by the use of phase-shift control, whereby very high frequency phase-shifted voltages are applied to the top and the bottom electrodes. Under these conditions, the shape of the distribution of ion fluxes can remain uniform across a broad range of processing working pressure and applied RF power conditions.[98]

2. External substrate scheme

In these reactor configurations, the plasma is generated by the use of an external plasma source, and the substrate is not a part of the plasma generating circuit. Still, the magnetic traps can be applied successfully to control the energy and density of ion fluxes, and the magnetic fields are generated between the plasma source and the substrate. As such, separate control of the ion current density to substrate and ion energy is possible by the use of PIII&D.

a. Array of ferromagnetic enhanced inductive plasma sources. One of the key limitations of CCPs operated at the driving frequency of 13.56 MHz lies in the challenge to generate sufficient plasma densities at low working pressures. Application of higher RF powers does not lead to a considerable enhancement in plasma generation. Rather, the additional applied energy mainly contributed to ion acceleration. Among potential solutions, inductively coupled plasma source enhanced with ferromagnetic cores (FMICP) can be used to generate high-density, uniformly distributed plasmas over large-area substrates.[99] Further improvements in high speed, large-area, uniform processing were achieved by employing arrays of RF couplers fitted with ferromagnetic cores.[100] An example of such a distributed FMICP source is shown in Fig. 13.

Here, the device consists of an inner and the peripheral arrays of toroidal couplers, at 6 and 12, respectively, which are housed in a holder designed to separate the plasma reactor into two sections [Fig. 13(a)], essentially forming two sub-reactors. The plasma is sustained by plasma current flowing in the opening of adjoining toroidal couplers. By controlling the distance between the coupler housing unit and upper flange, with all couplers in a series, it is possible to attain plasma distribution with considerable uniformity. Another approach to obtain similar uniformity of plasma profile can be attained by flowing distinct currents through individual arrays from unconnected power sources or from a single power source using a distributor.

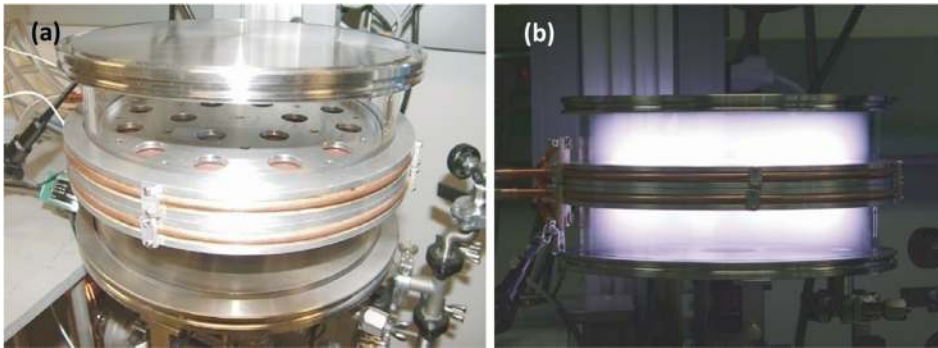

FIG. 13. Top (a) and side (b) view of inductively coupled plasma (ICP) source enhanced with ferromagnetic cores (FMICP) featuring eighteen distributed couplers. By driving distinct currents in individual coupler arrays from discrete power sources, it is possible to control ion current radial distribution and thus the shape of plasma. Reprinted with permission from Godyak *et al.*, J. Phys. D: Appl. Phys. **46**, 283001 (2013). Copyright 2012 IOP.

b. Array of helicon plasma sources. A different approach to improve the density and uniformity of plasmas is based on distributed RF excitations of inductively coupled plasmas by means of multiple antennas owing to remarkable efficiency of helical sources.[101] Helicon waves belong to bounded whistler waves, the right-hand circularly polarized electromagnetic waves. These waves can be described by the basic dispersion relation as[102]

$$\beta = \frac{\omega}{k}\frac{n_0 e \mu_0}{B_0}. \tag{14}$$

For an assumed operation mode, the density of plasma n_0 is proportional to magnetic field B_0. By employing multiple small sources organized into arrays, it is possible to generate sufficiently large-area plasmas for processing of large substrates, whereas the use of permanent magnets significantly reduces the complexity of the helicon sources. Figure 14 shows an example of such a design, where an eight-tube array is used to produce uniform discharge from processing of substrates with the area of up to $53 \times 165\,\mathrm{cm}^2$.

c. External substrate scheme: Neutral loop configuration at the plasma generation region. By controlling the diameter and position of the plasma ring relative to the substrate, it is possible to realize a time-averaged uniform distribution of a processing ion flux along a substrate. To achieve this control, a neutral loop discharge plasma method is used, where three coils are arranged around a processing chamber.

The top and bottom coils are powered to form a mirror-type stationary magnetic field, while the middle coil is powered to generate the magnetic field opposite to that generated by the top and bottom coils, thus generating the neutral magnetic loop.[103,104] RF power of 13.56 MHz is applied to an antenna coil wound outside the quartz vessel, and the coil is concentric with the neutral loop.

Thus, the RF electric field is induced azimuthally to the neutral loop and generates plasma in the presence of a background gas. When applying the RF power, a plasma torus is formed with a radius somewhat smaller than that of the neutral loop. By changing the middle coil current, the plasma ring radius is controlled (it is reduced as the current increases). Furthermore, under the bias applied to a substrate in CF_4 neutral loop discharge plasma, the energetic electrons are attracted to the substrate from the neutral loop, producing CF_3^+ ions in a CF_4 neutral loop discharge.[105] Figure 15 presents the results of simulations of time-averaged spatial distribution $P(r, z)$ of the ionization collisions that produce CF_3^+ ions and distribution $I(r)$ of the ion flow on substrate as a function of the substrate bias. It can be observed that $P(r, z)$ expands toward the substrate along the downward separatrix under the bias.

The bias attracts not only CF_3^+ ions during its negative phase but also energetic electrons during the positive phase.

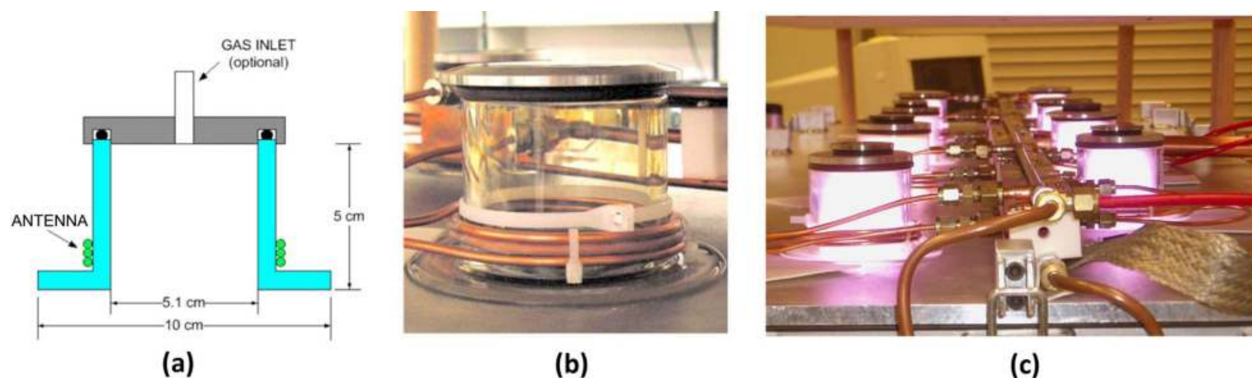

FIG. 14. Schematic representation (a) and physical appearance of plasma discharge reactor (b); an eight-tube permanent magnet helicon array powered from a rectangular 50 Ω transmission line (c).[101] This configuration allows for uniform processing of large-area substrates with plasma generated by arrays of small sources. The relationships between the discharge tube, the magnet, and the RF circuit are pivotal for device performance. Reprinted with permission from Phys. Plasmas **16**, 057102 (2009). Copyright 2009 AIP Publishing LLC.

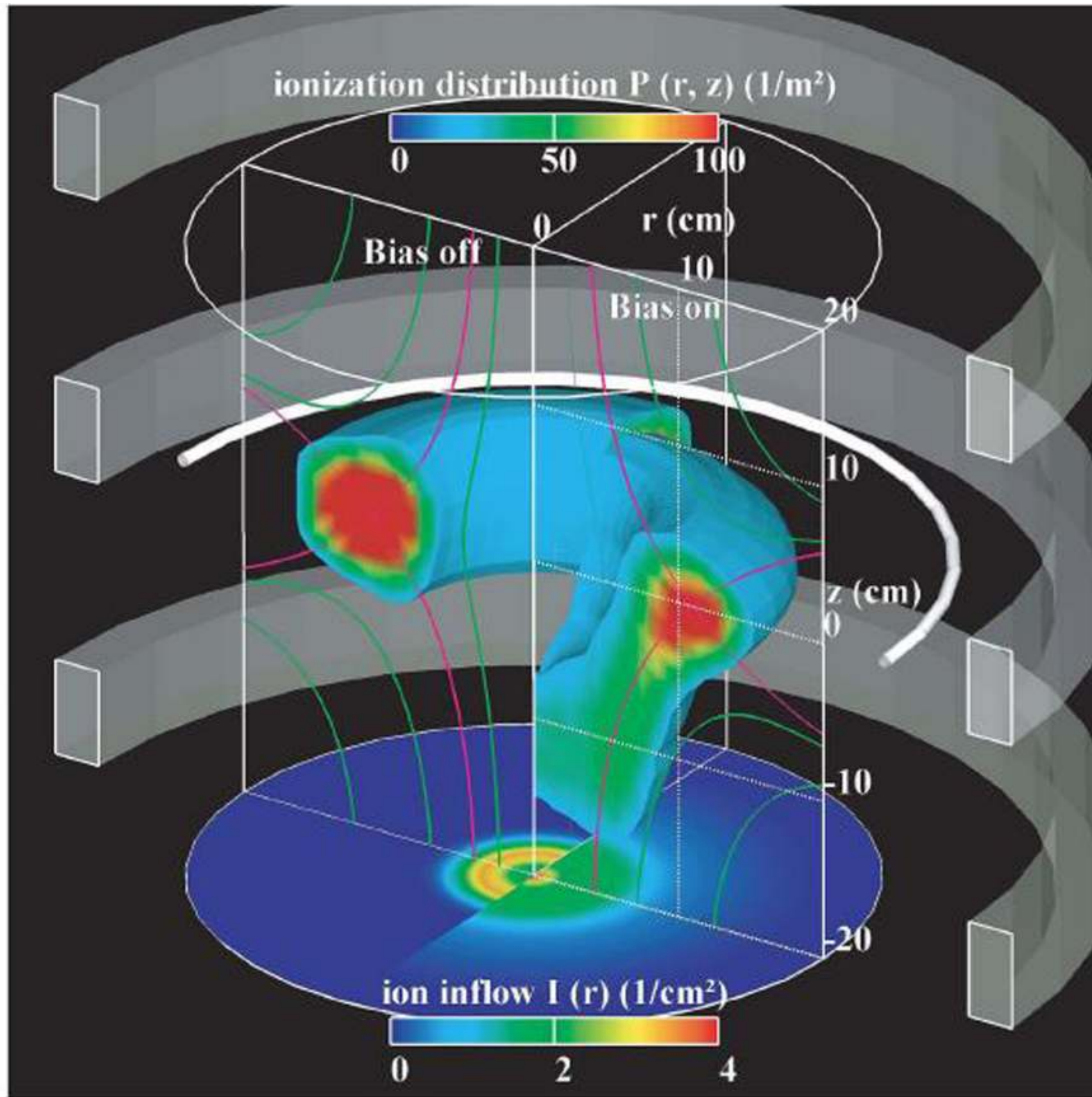

FIG. 15. Spatial distribution of dissociative ionization collisions, *P(r, z)*, producing CF_3^+ and ion inflow distribution, *I*(*r*), on substrate in the absence (left) and the presence (right) of substrate bias of 100 V. The green curves represent the magnetic field lines, the pink curves are separatrices of the quadrupole magnetic field, and the neutral loop is at the cross point of the separatrices. The bias drives the ion production region from the neutral loop toward the substrate along the downward separatrix. The ion flow to the substrate spreads and increases under the bias. Reprinted with permission from Asami *et al.,* IEEE Trans. Plasma Sci. **42**, 2540 (2014). Copyright 2014 IEEE.

The production of CF_3^+ ions increases due to electron heating by the bias. As a result, the region of production of CF_3^+ etchant approaches the substrate.

In the neutral loop discharge, the motion of a collisionless electron is described as

$$\frac{d\vec{v}}{dt} = -\frac{e}{m}\left(\vec{E} + \vec{v} \times \vec{B}\right), \tag{15}$$

where $\vec{v}$ is the electron velocity and $\vec{E}$ and $\vec{B}$ are the electric and magnetic fields expressed in the form:

$$\vec{E} = \vec{E}_0 \cos(\omega t + \varphi_0), \quad \vec{B} = \frac{B}{L}\begin{pmatrix} 0 \\ x \\ 0 \end{pmatrix}, \tag{16}$$

where ω and φ_0 are the driving frequency and the initial phase; L is the distance defined as the distance at which the magnetic field becomes B; the magnetic neutral plane is located at $x = 0$. Thus, the magnetic field is static, and the electric field is assumed as perpendicular to the magnetic field.

The average energy that electron gains from the electric field is given by

$$\varepsilon = \frac{\bar{x}_0^2 + 1}{2\left(\bar{x}_0^2 - 1\right)}\left(\frac{eE_0}{mL\omega^2}\right)^2, \tag{17}$$

where $\bar{x} = x/L$; the energy εdepends on the initial position x_0 and very large when $x_0 \rightarrow 1$.

d. Set of magnetic mirrors along the chamber walls. Multipole confinement illustrated in Fig. 10 is also widely applied for control of ion flux in the external substrate scheme. Set of magnetic mirrors (magnetic bucket) is

arranged along the vacuum chamber walls, which allows for the insulation of the plasma discharge from the walls of the reactor. This decreases the plasma loss and enhances the density of plasmas and that of the ion current to the substrate. Figure 16(a) shows an example of such setup for the enhancement of the power of the plasma, where RF inducted plasma is enhanced by the multipole confinement.[106] Figure 16(b) shows an inductive discharge system where, in addition to the enhancement of the discharge power, the plasma losses to a vacuum chamber walls are minimized using a combination of permanent magnets and external Helmholtz type electromagnetic coils, which are located outside the discharge reactor.[107] In this setup, the axial magnetic field is adjusted so the plasma is weakly magnetized. A grounded grid is inserted to separate the processing chamber into two parts, a plasma diffusion region (above the grid) and an ion extraction region (below the grid). A positive grid bias up to 70 V is applied to the grid, and it is observed that the plasma ion density increases with the bias voltage when no magnetic field is applied. Hence, a positive grid bias voltage enhances the plasma discharge in unmagnetized plasma. When an external magnetic field is applied, the plasma ion density decreases with the bias voltage less than 30 V and then increases at the bias larger than 30 V. The plasma density decreases by 3 times at the minimum bias of 30 V.

It is suggested that as the plasma density decreases, the electrons are drawn from the plasma along the magnetic field to the grid and ions are rapidly repelled toward the chamber wall. As the potential increases, the potential difference between the anode grid and the plasma cathode may exceed the ionization potential of the background gas. Under these conditions, the glow discharge is formed, contributing to the increase in the plasma density. Thus, the plasma ion density can be adjusted with no change in the source plasma flux. Yet, the distribution of the ion current along the substrate is not affected in this schematic. For the multipole confinement, in a case when a is the distance between the magnets that is much larger than a width w of the magnet, the magnetic field midway between the magnets ($x = 0, \pm d, \ldots$) is zero at the substrate surface ($y = 0$) and rises to a maximum above the chamber walls at $y = 0.28d$:3

$$B_m = \frac{\pi^2}{8}\frac{w^2}{a^2}B_0, \tag{18}$$

and then decays exponentially with y.

To describe the fraction f_{loss} of plasma that is lost through the magnetic cusps arranged along the chamber of radius R

$$f_{loss} = \frac{w_{leak}}{a}, \tag{19}$$

the effective leak width w_{leak} is used that is described for very low pressure

$$w_{leak} \approx 4(r_{ce} r_{ci})^{1/2} \tag{20}$$

and

$$w_{leak} \approx \frac{2a}{\pi}\left(\frac{r_{ce} r_{ci}}{\lambda_e \lambda_i}\right)^{1/2}, \tag{21}$$

for intermediate pressure, where r_{ce} and r_{ci} are Larmour radii of the electron and ion near the wall at the cusp location and λ_e and λ_i are the electron and ion mean free paths.

e. Multi-slot antenna and external magnetic field to control microwave plasma. Yasaka *et al.* proposed a multi-slotted planar antenna as a means to produce highly uniformly distributed microwave plasma discharges (Fig. 17),[108–110] where the antenna ensures uniform radiation, and the plasma is not influenced by eigenmode structures of surface waves. This provides an avenue for controlling the radial

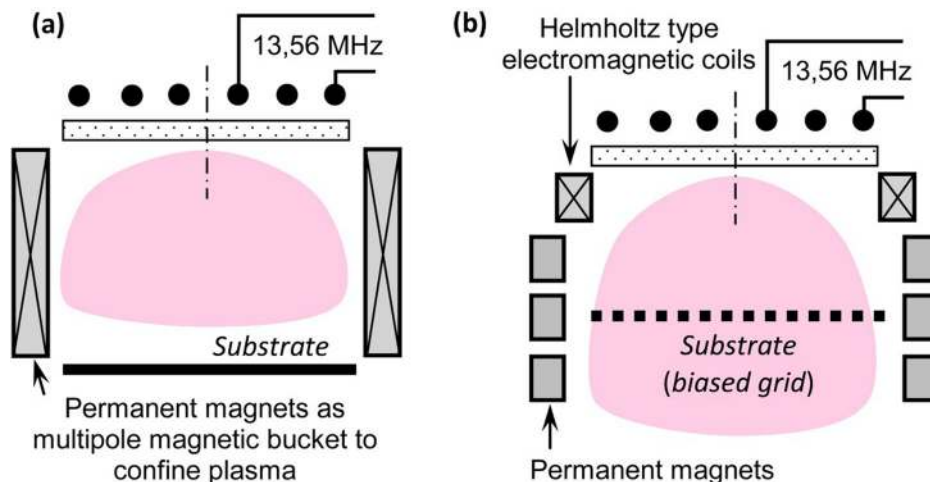

FIG. 16. Magnetic multipole confinement (magnetic bucket) in technological setups with the external substrate scheme: RF inducted plasma with multipole confinement to obtain the enhanced discharge power (a) and permanent magnets with external Helmholtz type electromagnetic coils outside the discharge chamber for the inductive discharge (b). The latter scheme allows controlling the density of ion current extracted from the plasma to the substrate, the latter being a grid: the electrons are drawn from the plasma along the magnetic field to the grid and ions are rapidly repelled toward the chamber wall at the positive bias increase up to 30 V, thus decreasing the plasma density; further increases in the potential lead to a glow discharge and associated increase in the plasma density.

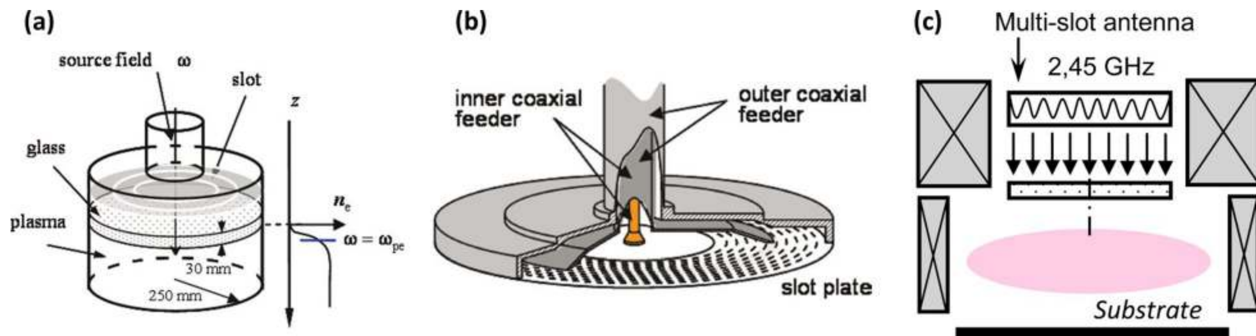

FIG. 17. (a) Schematic representation of a microwave plasma reactor. (b) The uniformity of the plasma is controlled by a segmented multi-slot planar antenna featuring inner and outer coaxial feeders. Reprinted with permission from Yasaka *et al.*, AIP Adv. 3, 122102 (2013). Copyright 2013 Authors, licensed under a Creative Commons Attribution 3.0 Unported License. By tuning power outputs of two microwave sources, it is possible to dynamically control the power absorption profile over large-area substrate (d = 300 mm, in this example). In the antenna, the space above the slot plate is separated into two radial sections, with a double coaxial feeder used to alter the balance of powers between the inner and outer sections, and thus control the radial distribution of radiation and plasma density. (c) An example of a large diameter ECR plasma setup.

distribution of the ion saturation current by changing the distribution of the power radiation and by changing the vertical position of the antenna. Thus-produced discharge can be used to effectively and uniformly treat the substrate of $\sim$700 cm^2.

In electron cyclotron resonance (ECR) plasma generated by applying an external magnetic field to the volume into which microwaves are injected, with the frequency of microwaves corresponding to the electron cyclotron resonance defined by the magnetic field, the resonant region is defined by the applied magnetic field rather than by microwave reflections. This enables the generation of large-area, spatially uniform plasmas, where an increase in the magnitude of the magnetic field is associated with the increase in full width at half maximum (FWHM) of the plasma density spatial distribution.[111] Figure 17(c) shows an example of thus-generated large-area ECR plasma produced with 2.45 GHz microwaves controlled by a multi-slot antenna and a TE_{01} mode microwave converter.

f. Open drift configuration: Magnetic mirror at the plasma generation region. When a magnetic mirror is arranged at the plasma generation region, the resulting magnetic field configuration facilitates the expansion of the plasma opposite to the magnetic field gradient [Fig. 18(a)].[112] In addition, magnetic coils can be arranged to pass the plasma through the inner diameter of the coils, thereby filtering the plasma and directing it to a particular area of a substrate [Fig. 18(b)].[113]

A number of configurations were developed, some of which are illustrated in Fig. 19. Unbalanced magnetrons, where the inner magnet is weaker compared with the outer magnet of the magnetron, have been proposed as an effective means to increase the density of the current of metal ions from the plasma generation region to the substrate [Fig. 19(a)]. Figure 19(b) shows a high power impulse magnetron sputtering (HIPIMS) system, where a magnetic coil is located in front of the target.[21] Figure 19(c) shows a setup, where a twist filter is responsible for the direction of the ion flux towards selected areas of the substrate in the vacuum arc deposition.[114] Here, the mechanical handling of the filter is used, which increases the complexity of this setup. Figure 18(b) shows the formation of the plasma lens created between a magnetron and a substrate, which has been demonstrated to effectively control the ion-to-neutral aspect ratio and thus the properties of the deposited thin film.[43] In an attempt to facilitate the deposition of uniform coatings over larger substrate areas, a plasma source incorporating a set of deflecting coils have been proposed [Fig. 19(d)].[115] Yet, this setup has limited utility for the production of focused ion fluxes directed toward a particular area of a substrate. Uniform plasma treatment was also obtained by use of the magnetic field bucket schematic shown in Fig. 19(e).[116] Here, a magnetic field similar to that of permanent multipole magnetic homogenizers is produced by putting a current through wires located on the inner wall of a cylindrical support structure.

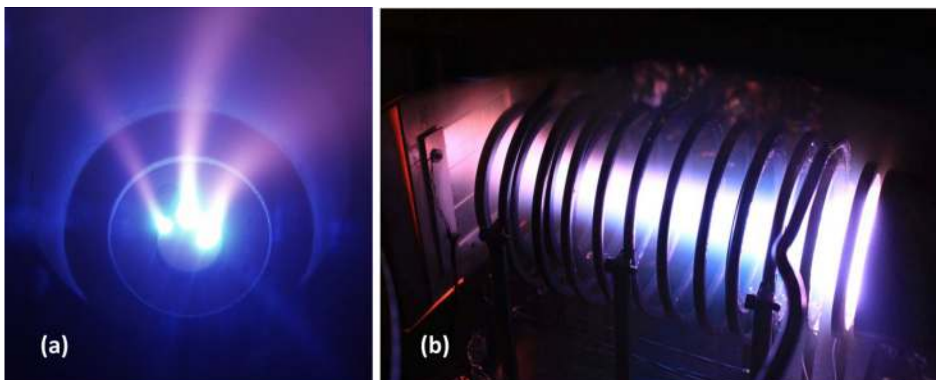

FIG. 18. Plasma expansion from a cathode of a vacuum arc source, where a guiding magnetic field is generated by the use of a coil mounted on a tubular plasma duct (a) (original photo by the authors) and plasma lens placed between (right) magnetron and (left) substrate, where the guiding magnetic field is generated by the use of an open filter configuration (b). Reprinted with permission from Anders *et al.*, IEEE Trans. Plasma Sci. **36**, 2528 (2011). Copyright 2011 IEEE.

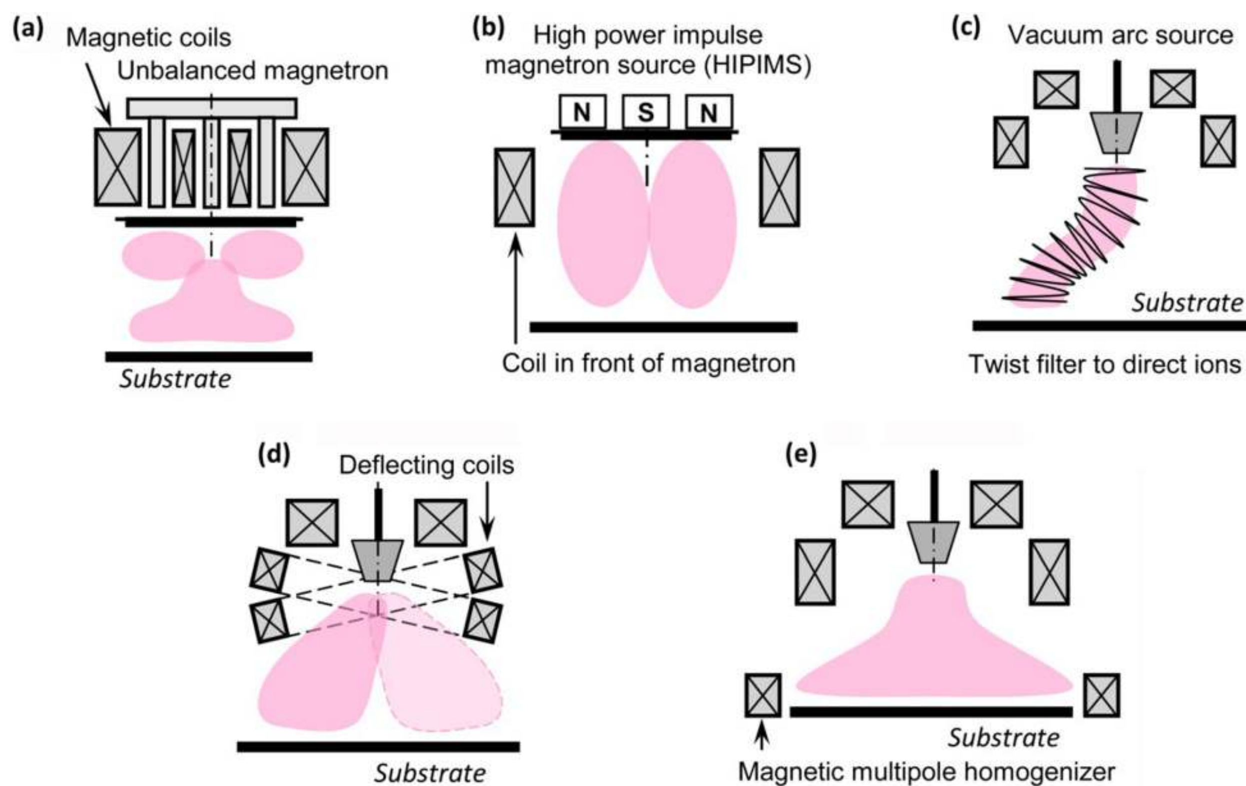

FIG. 19. Open drift configuration with a magnetic mirror in the plasma generation region: use of external magnetic coil to control confinement power in an unbalanced magnetron setup (a); same for the high power impulse magnetron source (b); twist open filter to remove microparticles from an arc discharge plasma (c); deflecting coils on a plasma duct to create time-averaged wide uniform distribution of the ion current density along the substrate surface (d); magnetic bucket above the substrate to make a more uniform distribution (e).

Thus-produced current-driven plasma homogenizer above the deposition plane enhances the uniformity of the radial density profile of vacuum arc metal plasma. These are just several examples of setups that can be used to control the plasma fluxes in a specific way. Yet, a flexible control that allows for selective generation of both wide and focused ion beams within the same setup is not possible with this approach, since the arrangement of the set of the magnetic coils defines the plasma configuration.

In contrast, the use of a set of magnetic mirrors allows for the flexible control of the plasma fluxes, as was demonstrated in the dual magnetron deposition setup shown in Fig. 20.[117] Here, when a magnetic bottle configuration is generated between the powered coils of the magnetron, plasma is located in the magnetic trap. However, if the magnetic cusp is formed between the magnetron, plasma is directed toward the substrate.

g. Systems incorporating two magnetic mirrors with perpendicular axes. The interaction of the magnetic mirrors similar to that shown in Fig. 20 has been investigated as a mean to control the shape of the discharge. Here, we describe a system that incorporates one set of the magnetic mirror-forming coils located in the plasma generation region (vacuum arc source), while another set of coils is placed under the substrate. In the simplest scenario, a single coil under the

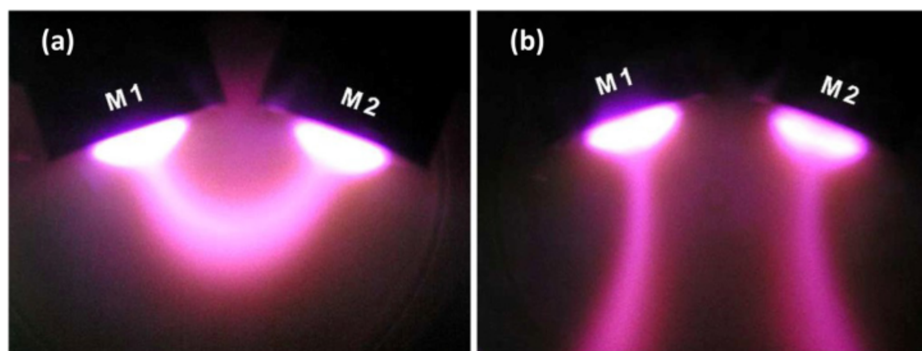

FIG. 20. Images of the plasma discharge generated in the dual magnetron system operated in a bipolar mode at repetition frequency of pulses 100 kHz, discharge current 0.5 A in nitrogen at pressure 0.5 Pa. (a) Closed magnetic field and (b) mirror magnetic field. By controlling the powering of the magnetic coils, it is possible to generate denser plasma in a magnetic bottle (a) or to direct the plasma flux toward the substrate by the use of magnetic cusp between the powered coils (b). Reprinted with permission from Musil *et al.,* RSC Adv. **5**, 60482 (2015). Copyright 2015 RSC.

substrate is used. Figure 21 shows one such configuration, where a magnetic mirror generated by the coil under the substrate is aligned transverse relative to the magnetic mirror in the arc source.[118]

Plasma discharge that was generated around the spherical target had plasma density of about $10^{17}\,\text{m}^{-3}$. The ion deflection along the magnetic field was enabled by the magnetized electrons compensating the space charge of the ion flux. The impact ionization of the background gas was facilitated by the electrons confined along the length of the plasma stream. At a pressure of or above 0.1 Pa, the target current was affected by the orientation of the magnetic field relative with respect to the plasma flux. These observations may provide valuable insight into the processes of plasma transport via the curved ducts, and the mechanisms that govern the interactions between plasmas and complex 3D objects.

The electron behavior within the plasma stream generated in Fig. 21 was examined to gain better understanding of the observed phenomena.

The magnetic field forces electrons to circulate along the magnetic lines, moving along the plasma stream. Concurrently, the transversal electrical field facilitates the diffusion of electrons to the stream periphery, forcing them toward the walls of the plasma reactor across the magnetic field. Furthermore, the drift motion of electrons, where they move across the plasma stream axis and across the transversal electrical field, also takes place. The latter motion facilitates the transport of electrons around the stream axis; however, its contribution is limited, whereas the electron motion to the walls of the deposition reactor enables the loss of the electrons from the plasma stream. Given that the mobility of electrons along the magnetic field is far greater than that across the field, the escape of electrons may be accompanied by oscillations along the length of the plasma stream. It is possible to quantify the electron movements along the plasma stream as

$$\eta_c = (1+\varpi^2)\frac{E_p}{E_t}\frac{\Delta}{l}, \tag{22}$$

where E_t and E_p are the electrical field across and along the stream, Δ is the stream thickness, and l is the distance along the plasma stream.

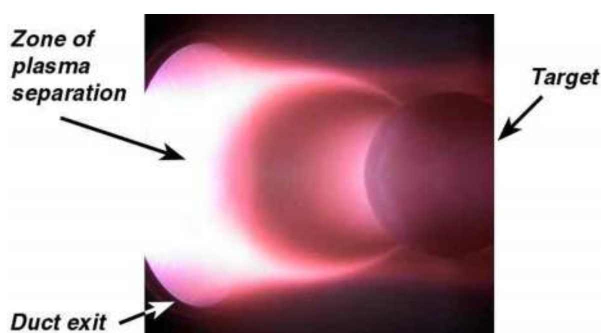

FIG. 21. An image of the arc plasma split into two streams at the duct exit and spherical target (left panel). Two magnetic lines are used to confine the plasma as it left the duct: an "external" magnetic line intersecting the duct shell, and "internal" line that intersects the duct axis at the duct exit plane. In the region between these lines, the plasma-generated elections are magnetized, and then obey the configuration of the magnetic field. This produces defined upper and lower plasma streams. The measured plasma density approaches $2\times10^{17}\,\text{m}^{-3}$and $2\times10^{16}\,\text{m}^{-3}$ in the proximity of the target surface and at the plasma duct exit, respectively. Magnetized electrons compensate the space charge of the ion flux, enabling the deflection of ions along the lines of the magnetic field. The electrons are confined along the stream length, providing impact ionization of the background gas. Structure of the spherical target is illustrated at the right panel. Reprinted with permission from Levchenko *et al.,* IEEE Trans. Plasma Sci. **32**, 2139 (2004). Copyright 2004 IEEE.

h. Magnetic mirror under substrate in line with magnetic mirror at the plasma generation region: Coaxial arrangement of electromagnets. A configuration depicted in Fig. 22, where the coil is mounted under the substrate transverse with a coil near the plasma source, enables the transition of the initial Gaussian distribution of the ion current density to a complex three-peaked distribution. When the coil under substrate is arranged coaxially with the coil of the plasma source, focusing of the ion current to the substrate center is possible. This scheme has been successfully integrated into a setup with the unbalanced magnetron.[22] Further modifications may include the use of an additional coil mounted under the substrate coupled with a mechanical attenuator.[119]

Two possible configurations can be obtained in a space between the powered coils:

(a) magnetic bottle when the coils are switched in-line, thus allowing focusing of the plasma to the substrate and controlling the ion-to-neutral aspect ratio. Particular disadvantage of the bottle configuration is its influence on the discharge parameters due to a reduction in the plasma electron mobility;
(b) magnetic cusp (circle mirror) when the coils are switched in an opposite manner, thus allowing filtering and directing of the plasma in a radial direction through the cusp. Ion loss through the magnetic mirrors can be considered as a disadvantage of this configuration when it is applied to focus the ion flux to the substrate.

As shown experimentally, when the substrate is processed by an ion flow in the presence of a neutral component of the plasma, the conditions of the surface layer formation strongly depend on the ratio α_{in} of the ion flow to the neutral flow, thus allowing to obtain qualitatively new characteristics of the surface.[120,121] When combining different plasma sources, it has been shown that the control of the ion current is possible. In the hybrid plasma setup, which combines the arc and planar magnetron, it is possible to produce a domain of dense plasmas with a narrow ion beam directed to a particular area of the substrate. An image of the magnetron discharge at the gas pressure of 0.5 Pa is shown in Fig. 22(a). The discharge has a ring structure conditioned by the arc-shaped magnetic trap for the electrons. Figure 22(b) shows the plasma structure produced by the arc source, when the planar magnetron is not operating (i.e., the magnetron discharge was not ignited, but the magnetic field of the magnetron was present). When both sources operate and the magnetic field of the magnetron is directed in-line with the field of the arc source, a bottle configuration of a magnetic

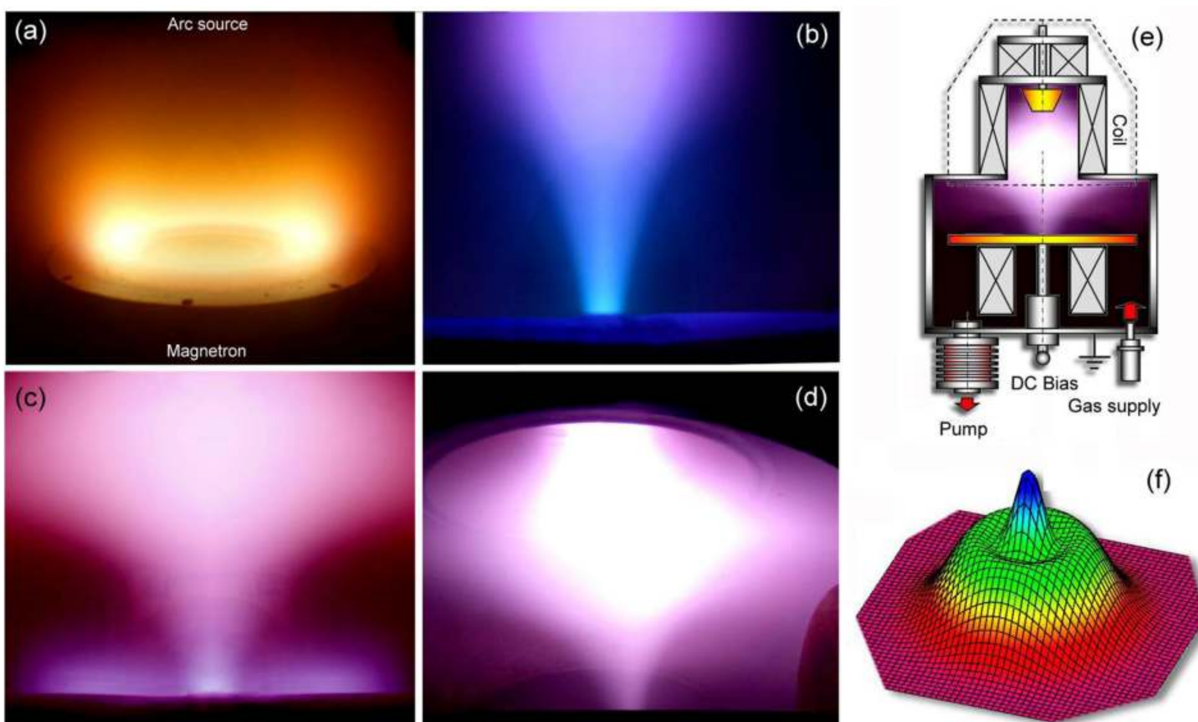

FIG. 22. Plasmas attained using different configurations of the magnetic traps. (a) Ring-shaped magnetron discharge generated in the arc-shaped magnetic trap. (b) Powerful jet generated by the bottle-shaped magnetic trap between the arc and the magnetron sources at a gas pressure of 0.02 Pa. (c) Tube-shaped plasma jet directed from the bottle trap to the arc-shaped trap. (d) Powerful jet with controlled ion-to-neutral flux ratio. (e) Schematic of the setup (rotated counterclockwise by 90° relative to the discharge photos). (f) 3D visualization of the measured distribution of the ion current over the substrate for the configuration in (d). Reprinted with permission from Baranov *et al.*, IEEE Trans. Plasma Sci. **42**, 2518 (2014). Copyright 2014 IEEE.

trap is formed between the arc source and the substrate. A domain with the excess of the plasma electrons over the ions is generated in the magnetic trap.

The ions are affected by a self-consistent electric field, and the plasma flow is focused to a narrow area located right above the magnetic pole of the magnetron, with the ratio α_{in} of 1. Increasing the gas pressure to 0.5 Pa changes the configuration of the plasma, as shown in Fig. 22(c). This change is attributed to the formation of another domain with the electron excess—in the region of the arc-shaped magnetic trap of the magnetron. The domain is formed by the bulk electrons, which are generated through the ionization of the residual gas by the secondary electrons emitted from the substrate. In this case, the ion flow is directed toward the magnetron trap, while $\alpha_{in} = 0.02$. At the intermediate pressures, the focusing of the ion flow at a fixed level of the gas pressure is possible. The discharge structure for the pressure of 0.1 Pa ($\alpha_{in} = 0.1$) is shown in Fig. 22(d), schematic of the setup is shown in Fig. 22(e), and the measured distribution of the ion current over the substrate is shown in Fig. 22(f). The parameter α_{in} was estimated by the technique described in detail elsewhere.[46]

i. Systems incorporating two complex magnetic mirrors with parallel axes. The configuration discussed in Sec. II C 2 h can be used to obtain a small set of possible distributions of the ion current density along a substrate, thus limiting a flexible control of the ion fluxes. To overcome this limitation, a set of coils with axes parallel to the axes of plasma-generated magnetic system can be installed under the substrate.[122] The feasibility of this approach is illustrated in Fig. 23, where the plasma flow is effectively controlled by changes in coil configuration.

In comparison with the initial shape of the discharge illustrated in Fig. 23(a), Fig. 23(b) shows the formation of the plasma jet that preferentially targets the periphery of the substrate under which the corresponding magnetic coil is housed. Whereas, in Fig. 23(c), the vacuum arc plasma discharge is focused at the central zone of the substrate, with the configuration obtained without changes to the operation mode of the source. In Fig. 23(d), distributed plasma flux lacking a single focus is produced and is directed toward the periphery of the substrate, below which the opposite powered coils are located. The probe measurements confirm the resultant change in the ion current density distribution from the Gaussian-like to the horseshoe-shaped or the complex multi-peaked distributions.[80] The properties of the thin films fabricated under different plasma modes showed their dependence on the use of the additional coils.[123]

By locating the magnetic coils in the close proximity to each other and powering them in line with the coils near the plasma source, it possible to generate two magnetic bottles within the chamber volume. This leads to the splitting of the plasma stream generated into the arc discharge into three distinct streams emanating from the substrate [Fig. 24(a)].[71] Here, the magnetic cusp which forms between the coils controls the narrow plane-shaped plasma stream, whereas the magnetic poles of the coils located under the substrate govern the behavior of the two side plasma streams. Thus-obtained configuration of the resultant magnetic field is

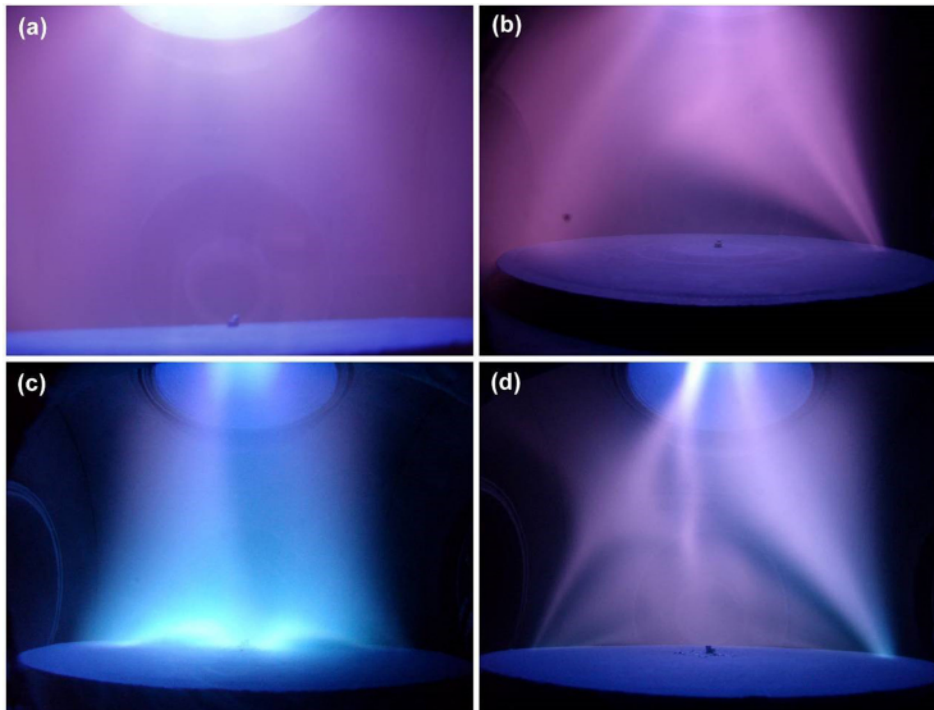

FIG. 23. Images of possible plasma structures obtained using vacuum arc plasma source under different configurations of the magnetic field: only coil of the plasma source is powered (a); coil of the plasma source and right coil under the substrate are powered in-line to form a magnetic bottle between them (b); each of the coils under the substrate is powered in-line with the coil of the plasma source (c); right coil under the substrate is powered in-line with the coil of the plasma source while the left coil is powered opposite to form a cusp configuration between the left coil and the coil of the plasma source, magnetic bottle is formed between the poles of the left and right coils to prevent the plasma penetration to the substrate center (d). Reprinted with permission from J. Appl. Phys. **112**, 073302 (2012). Copyright 2012 AIP Publishing LLC.

suitable for the plasma focusing to the area located between the coils, with a strongly time-averaged focused ion beam obtained for a rotating disk-shaped substrate.

As discussed earlier, powering of a single coil results in the formation of a single powerful jet, which can be sustained and effectively deflected to the magnetic pole of the powered coil. As the background gas pressure increases, the focusing becomes less clearly defined, as shown in Fig. 24(b), and then virtually disappears at a pressure of 1 Pa.[124] In the case when one coil is powered in line with the coils near the plasma source, while another one is powered oppositely, the resulting magnetic field protects the central part of the substrate from the plasma penetration, since the plasma is effectively transported toward the peripheral areas of the substrate. Indeed, with the use of auxiliary under-substrate magnetic coils, it is possible to selectively isolate the areas of treatment and material deposition. Figure 24(d) shows the distribution of the material density across the surface of the

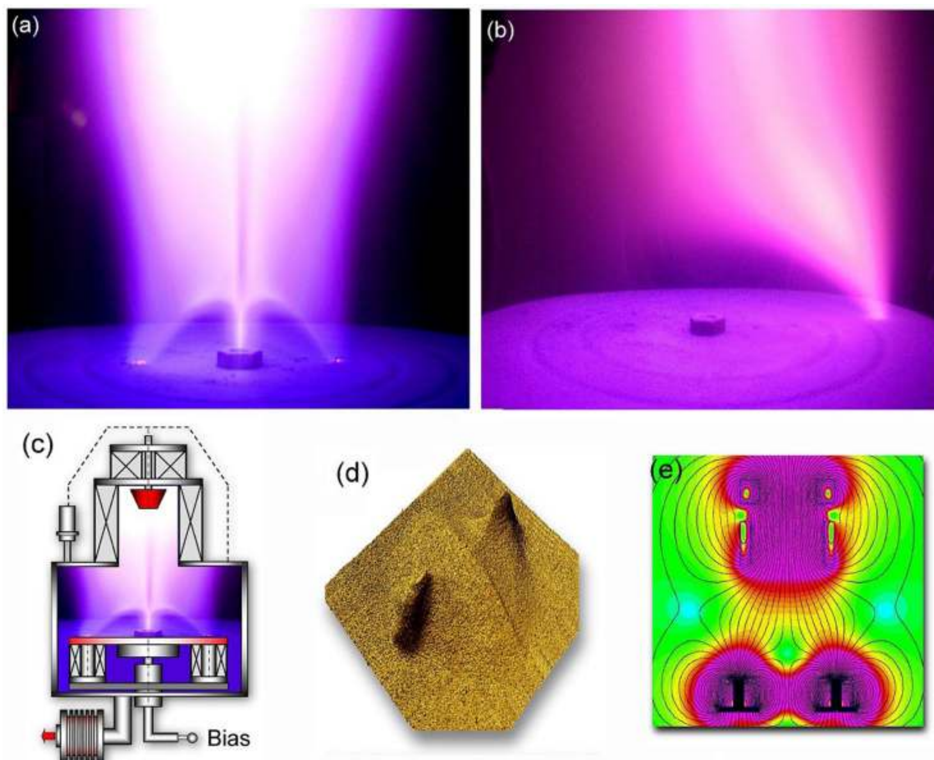

FIG. 24. Formation of complex arc discharge plasma stream patterns under two configurations of the magnetic coil system. (a) Plasma stream is split into three streams attached to the substrate. (b) A single powerful stream is sustained and effectively deflected to the periphery of the substrate. (c) Schematic of the arc discharge setup. (d) Representative 3D visualization of the density of material deposited on the surface of the substrate under two-stream plasma.(e) Calculated topography of the magnetic field for the setup shown in (c). Reprinted with permission from Baranov *et al.*, IEEE Trans. Plasma Sci. **42**, 2464 (2014). Copyright 2014 IEEE.

substrate under two-stream configuration. Figure 24(e) shows a corresponding topography of the magnetic field calculated for the setup shown in Fig. 24(c).

Industrial plasma setups typically employ both the arc and bottle configurations of the magnetic field, the choice being governed by the demands and limitations of specific technological process. In application where etching, modification, or heating of the surface layers by gas ions is required, such as for surface cleaning or preparation for subsequent film deposition, the arc configuration is most appropriate. On the other hand, while the bottle configuration in conjunction with PIII&D can be used for similar processes, it is also suited for the metal and gas ion-based synthesis of micro- and nano-structures.

When the system is operated in ESS mode discussed in detail in Sec. II C 2 f, bottle-shaped magnetic fields can be used to trap plasma electrons and govern the movement of ion fluxes generated by an external plasma source.[122] To enable effective injection of the plasma-generated species into the traps, the magnetic mirrors of the traps should be placed in the proximity of the plasma source, whereas for the best control over the ion fluxes to the surface of the substrate, they should also be located above the target substrate. Practically, this can be achieved by mounting the electromagnetic coil near the inlet of processing reactor, between the plasma source and the reactor. Furthermore, a set of magnetic coils should also be located under the substrate to control the shape of thus-generated magnetic field (see Fig. 24).

The shape of the field will govern the formation and distribution of negative space charge regions in the plasma.[122] In Secs. II C 2 f–II C 2 h, the formation of bottle and cusped magnetic fields and ensuing formation of the magnetic traps for the plasma electrons have been discussed.[125] It is important to stress that unlike the electrons, ions are not confined by these magnetic fields, which leads to high electron density and consequently negative electric space charge within the traps. Thus-produced negative space charge influences the behavior of plasma-generated ions as they enter the processing chamber from the plasma duct. Therefore, although the magnetic trap itself does not affect the kinetic energy E_{ion0} of the ions as they traverse the trap, their motion is affected by the negative space charge from the accumulated electrons. The resultant changes in the ion motion can be described using a theoretical approach of plasma optics.[126] The approach views the traps as charged volumes of spherical geometry, with the relationships between the radius of the sphere and the electric potential described as $\varphi(r) = Ar^2$, where A is a constant. With the ions viewed as particles in a central field, their motion is then defined by a series of motion equations.[122,127]

The electrons are assumed to be distributed uniformly within the volume of the magnetic trap, with the electron density being independent from the radius of the sphere. Considering this assumption, an excess of electrons to ions of approximately 10^{-5} would result in the formation of an electric field of the strength (up to 500 V/m) sufficient to have a significant effect on the trajectories of ions as they traverse the volume of the traps, and their distribution over the surface of the substrate.[122]

Since the shape and the magnitude of the resultant magnetic trap will be affected by the arrangement of coils used to generate individual magnetic fields, e.g., those located underneath the substrate and in between the plasma source and the inlet of the reactor, application of the power to these magnetic coils presents an important means for the control over the treatment process. Indeed, given the significance of self-consistent electric fields formed within magnetic traps by magnetized plasma electrons in controlling the motion of ions as they traverse the traps and are directed towards the substrate, such a method of control over the gas and metal ion fluxes and their interaction with the large-area surfaces at distinct stages of ion treatment can bring significant benefits.

The ability to sequentially alter the shape of the plasma and thus the distribution of the ion fluxes over the surface of the substrate by magnetic field is particularly attractive. Thus-produced time-averaged ion flux distribution is the result of the superposition of the individual distributions, the statistical weights of which are derived from the relative duration of the plasma treatment under each magnetic field configuration. Considering the shape of these individual distributions of the ion fluxes to be Gaussian-type, the time-averaged distribution can be defined by the expression:

$$\overline{J}(x,y) = \frac{1}{t_\Sigma}\sum_i^n t_i\left(\sum_j^m J_{0ij}\exp\left[-\left(\frac{(x-x_{0ij})^2}{\Delta x_{ij}^2}+\frac{(y-y_{0ij})^2}{\Delta y_{ij}^2}\right)\right]\right), \tag{23}$$

where t_Σ is the total time of the substrate processing; t_i is the time of the plasma exposition to the ith configuration of the magnetic field; J_{0ij}, x_{0ij}, y_{0ij}, Δx_{ij}, and Δy_{ij} are the parameters of a distribution of j-component of i-distribution.

The range of these individual distributions in Eq. (23) can be extended by considering the effects of the control magnetic fields on the properties of the plasma, and movements of the magnetic field in relation to the plasma.[80,122]

The flexibility of the system partially discussed in Secs. II C 2 f–II C 2 h, is illustrated by the experiment, where it was used for the entire fabrication process, from substrate preparation, to synthesis of wear-resistant thin films on the surfaces of cutting tools. Figure 25 shows possible operation modes that can be attained using this experimental setup. Briefly, for the substrate preparation, namely, surface cleaning, chemical functionalization, and production of the underlayer, the ISS mode is used. For the formation of the transition layer and synthesis of the coating, ESS with metal plasma of the vacuum arc source is used. At a low gas pressure, dense, fully ionized plasma discharge is generated by the vacuum arc plasma source. For the characteristic operation mode, under these conditions the confinement of plasma electrons due to the effect of the background gas is insignificant and can be ignored. Operating in ISS mode, the ion fluxes can be effectively controlled by the closed drift of electrons, which are confined by the presence of the arc-shaped magnetic field above the substrate.[80] The magnetic field was produced by cylindrical electromagnet. To provide for addition flexibility, the inner and outer sections of the magnetic core were detachable.

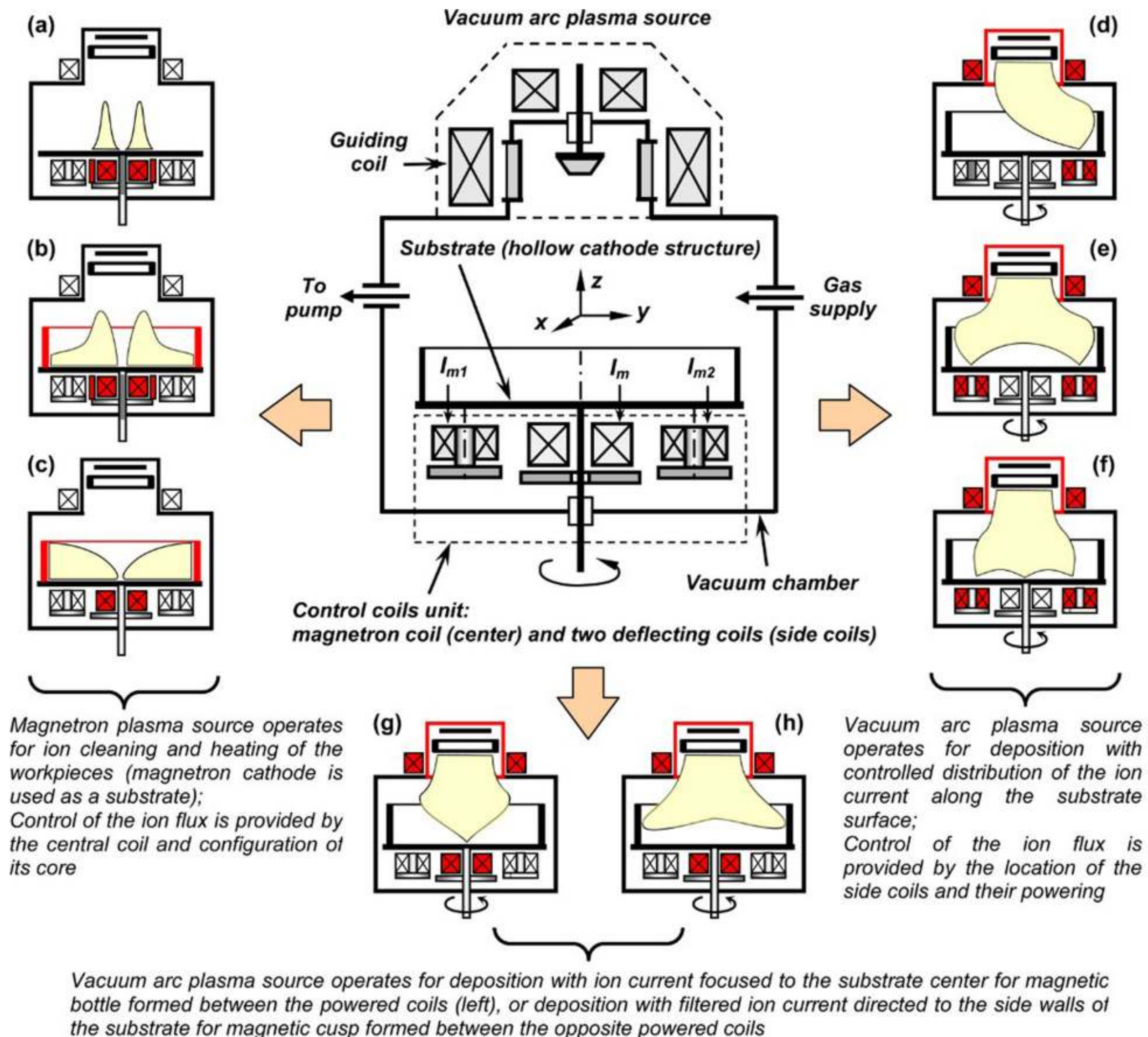

FIG. 25. Possible operation modes of a system, which uses under-substrate magnetic mirrors and a magnetic mirror at a plasma generation region to control ion fluxes. The left panel illustrates possible operation modes for the ISS, where the shape of the plasma discharge is controlled by (a) the magnetic core configuration, (b) the addition of the hollow-cathode structure, and (c) powering of the central coil. Alterations to the arrangement of the magnetic core leads to the increase in the radius of the magnetic field lines, thereby affected the width of the ion flux distribution over the substrate. The hollow-cathode structure guarantees the discharge ignition by enabling the contact between the magnetic field lines to the biased surface. The strength of the magnetic field and the power of the plasma discharge are related to the power supplied to the central magnetic coil. The right panel illustrates possible operation modes for the ESS. Here, the shape of the plasma is governed by (d) altering the spatial arrangement of the control magnetic coils located under the substrate, and (e) and (f) by powering of the set of the control coils (installed at the inlet of vacuum chamber between the plasma source and the chamber and under the substrate). The characteristics of the magnetic field that result from the superimposition of the individual magnetic fields are determined by the strength and direction of the latter. Therefore, the manner in which these coils are powered provides an effective means for the control of the magnetic field configuration. The central panel shows schematic of the experimental setup. The bottom panel also shows operation modes for the external substrate scheme where plasma is controlled by (g) changing the resulting magnetic field to a bottle configuration between the in-line powered coils, thus allowing focusing the plasma flux with a purpose of controlling ion-to-neutral ratio,[22] and (h) changing the resulting magnetic field to a cusp configuration between the opposite powered coils, thus allowing focusing the plasma flux with a purpose of deposition of the filtered ion flux to a side surfaces of the substrate.[115]

As the substrate, a thin, stainless steel hollow-cathode structure was affixed to the rotating table above the said cylindrical electromagnet to tie the magnetic field lines to the surface of the substrate, which was negatively biased with respect to the grounded walls of the plasma reactor. This solution allowed for the guaranteed ignition of the magnetron discharge in the proximity of the substrate. Under ISS mode, the substrate performed the role of a cathode in the plasma-generating circuit.

When operated in ESS configuration, bottle-type magnetic traps were produced with the aim to govern the ion fluxes generated by the vacuum arc plasma source to the surface of the substrate. The plasma source consisted of the Ti cathode and an anode. The stream of plasma was directed toward the surface of the substrate by means of the magnetic field, which reached $B_g = 0.016\,\mathrm{T}$ at the center of the guiding coil. The anode, onto which the guiding coil was affixed, performed the function of a plasma duct, whereas the

guiding coil located between the plasma source and the inlet of the processing reactor formed a part of the magnetic control system. The substrate was located in a way that its center was aligned with the axis of symmetry of the duct. The distribution of the plasma current density along the x and y axes of the surface of the substrate was obtained using a planar probe.[128–130]

When used for TiN deposition, this system was operated in the ISS closed drift configuration at the plasma generation region (Sec. II C 1) in combination with electrostatic confinement based on a hollow cathode scheme (Sec. II B 1) for the operations of ion cleaning and substrate heating, whereas the ESS with a set of magnetic mirrors under substrate and magnetic mirror at a plasma generation region was used for the deposition (Secs. II C 2 f, II C h, and II C 2 i).

III. PRACTICAL EXAMPLES: APPLICATION FOR MICRO- AND NANOSYNTHESIS

In Sec. II, the effect of the magnetic field on the energy and motion of charged species have been considered. In this section, a select number of cases will be examined to explore the effects of the ion energy and ion flux on the structure and characteristics of the thin films synthesized using the aforementioned plasma systems. Indeed, it is well-known that the properties of the materials fabricated using plasmas under low ion energy and strong ion fluxes and those produced under high ion energy[131,132] but low ion flux[30,133] are likely to be quite dissimilar. Given that the ion current is affected by the process temperature, the latter will also have a profound effect on the characteristics of the thin films.[134,135] By manipulating the ion current density, it is possible to produce films with uniform properties across the entire substrate,[18,136] as well as thin film structures in which the characteristics are varied across distinct areas of the substrate.[135,137,138] Even though structure zone diagrams may provide useful quantitative insight into to the effect of ion current density on the resultant characteristics of the treated surface, they are unable to adequately account for all aspects of the behavior of the material. One of the key complexities arise from the fact that most systems present a unique combination of a substrate, deposit, and processing conditions that can differ in a variety of ways, and it is therefore impossible to devise a SZD that would be able to accurately predict the experimental outcomes.

Let us now consider the first example of the plasma system where magnetic field is used to control the ion fluxes. The magnetron–ICP system comprises a steel processing reactor ($V \approx 0.25$ m^3). The temperature of the substrate holder can be controlled using an in-built heating/cooling system. The plasma is externally generated using an RF coil mounted over the glass cylinder ($d = 120$ mm and $h = 250$ mm), which is turn joined to the top metal lid of the processing reactor. Magnetic field is generated using two cylindrical magnetrons fitted with several metal targets. The gas is delivered into the processing chamber by means of a gas supply system, which allows for the control of the flow rates of the processing gases and their mixtures. Vacuum pump is used to lower the base pressure, monitored using Penning and Pirani gauges. To maximize the transfer of the energy from the RF generator to the plasma source, a matching capacitance L-type network is used. The RF generator has a maximum power output of 1 kW (28 MHz). The magnetrons can be used individually or in conjunction with the RF plasma-generating system. Figure 26 shows an image of the plasma discharge produced by a single operating magnetron (located on the left side of the image) and the RF source (at the top).[139]

The types of nanostructures that can be produced within this flexible system are diverse. For instance, in a mixture of Ar, H_2, and N_2 at 1000 W, nanostructures produced within this system on the p-type B-doped Si substrate are tree-like, as shown in Figs. 26(a) and 26(b).The synthesis was rapid, taking only 15 min, and did not require the use of the external heating, as the plasma-generated heating was sufficient to elevate the temperature of the substrate to 600 °C. The flux rates were kept at 20:10:2 cm^3 m^{-1} for Ar:H_2:N_2, and the substrate was kept under the bias of −150 V. Under microwave plasma conditions when the magnetrons are not used, the nano-flowers of multiwall carbon nanotubes were synthesized on the surfaces of Si (100) wafers, their structure shown in Fig. 26(c). As a processing gas, a mixture of CH_4 carbon precursor and N_2plasma-generating gases was used, with proportion of CH_4 varied from 10% to 80%. The deposition pressure was kept at 20 torr, and the synthesis was performed in the absence of external heating, as plasma-generated heating effects were sufficient to maintain the temperature of the surface at 700–800 °C. The synthesis was rapid, at 5 min, producing vertically oriented, several μm-long carbon nanotubes arranged in the clusters with the high surface density of ~250 CNT/μm^2. Slightly longer processing (of 30 min) was required to produce ZnO nano-belts [shown in Fig. 26(d)] from the Zn powder using an Ar/O_2 gas mixture. The respective ion fluxes of Ar and O_2 were kept at 50 and 14 cm^3 m^{-1}, the substrate temperature reached 800 °C, and the gas pressure was maintained at 40 mbar.

Structures produced by this advanced low-temperature plasma system include a variety of surface-bound metallic, oxide, and carbon nano-structures, e.g., vertically oriented graphene nano-flakes and carbon nanotube forests, which are needed for the advancement of nano-scale electronic, mechanic, medical, and energy devices.[140] For many of these devices, high quality, uniform treatment, and deposition over substrates with large surface areas are necessary. This can be easily achieved in this system by de-focusing the plasma over the entire surface of the substrate. However, it must be noted that the average current density in the de-focused plasmas is relatively low, which may negatively affect the quality and subsequently performance of thus-produced materials. On the other hand, generation of focused beams of plasma can deliver high-density ion fluxes to the specific areas of substrate, facilitating rapid synthesis of high-quality thin films and nanostructures and enabling processing of multiple wafers within a single process cycle. Yet, thus-focused beams have significantly smaller area that can receive treatment at any moment in time. Therefore, for industrial applications, there is a need to optimize the

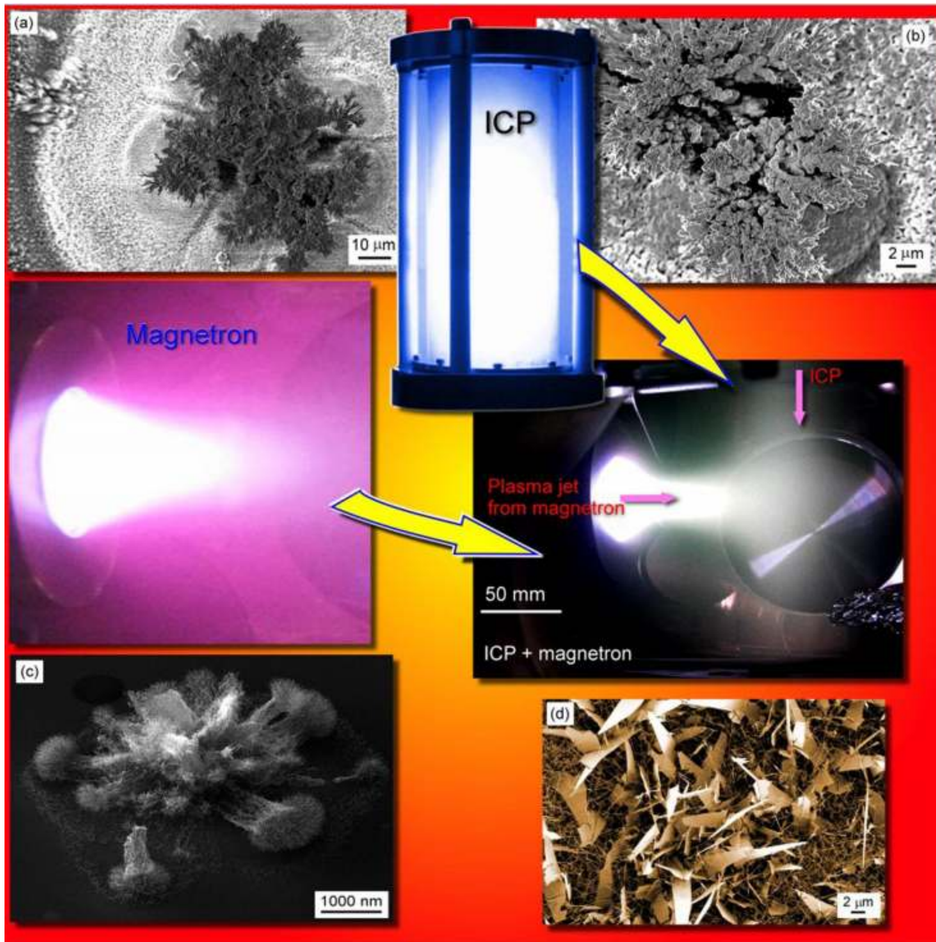

FIG. 26. Some of the possible nanostructures that can be produced in the advanced plasma-assisted system comprising the (top) RF ICP and (left) dc magnetron discharges. Central image shows a complex plasma configuration produced when the left magnetron and ICP source are operated. (a)-(d) Representative SEM visualizations of nano-flowers of carbon nanotubes, ZnO nano-belts, and Si nano-trees produced under different plasma configurations. (a) and (b) Si nano-trees grown in an $Ar + H_2 + N_2$ ICP plasma at an RF power of 1000 W. (c) a nano-flower of CNTs synthesized on a Si wafer using a microwave plasma. (d) a nano-flower of ZnO nano-belts synthesized using an $Ar + O_2$ gas mixture. Reprinted with permission from Ostrikov *et al.*, IEEE Trans. Plasma Sci. **39**, 2796 (2011). Copyright 2011 IEEE.

process to maximize both the ion current density and the processing area.

Let us consider an example, where vacuum arc deposition of TiN thin films on the surfaces of cutting tool inserts is optimized to produce dense, defect-free coatings by controlling the ion current density (Fig. 27). Plasma discharge was generated by applying dc arc current $I_a = 100$ A between the cathode and the grounded anode.

Magnetic field produced by focusing coils ($B_f = 0.03$ T) was employed to maintain the cathode spots on the surface of the cathode, whereas guiding magnetic field ($B_g = 0.016$ T) directed the plasma stream toward the treated substrate ($r = 200$ mm and $d = 8$ mm), which was kept at a negative potential of -200 V with respect to the grounded reactor walls. The deposition was performed in N atmosphere at 0.1 Pa for 30 min.

Plasma-cleaned and pre-heated cutting tool inserts were arranged at points $r = 0$, 40, 70, 100, 130, and 160 mm on the substrate surface. Once deposited, the coatings underwent rigorous testing, e.g., by using coated tools for lathe machining of very hard and strong AISI 431 steel used in many important industrial applications.[141] The tools were then evaluated for wear, assuming the critical wear criterion to be 0.4 mm.[45]

To understand the relationship between the ion current and the wear resistance of thus-produced coating, a planar probe was used to collect the distribution of ion current $J_i(r)$, the latter having a Gaussian-type shape, with r being the coordinate corresponding to the location of the samples of the substrate surface. The radial distribution of $J_i(r)$ was found to be significantly non-uniform. Similar approach was used to approximate the distribution of the measured film thickness $h_c(r)$, which was also strongly non-uniform. It is interesting to note that 2.1-time decrease in J_i led to a 1.8-time reduction in the film thickness, indicating a continuing departure between the $J_i(r)$ and $h_c(r)$ dependencies on radius r[45] and non-linear dependence of $h_c(r)$ on $J_i(r)$.

Visual examination of TiN films shows significant differences in the wear behavior of films deposited at different points on the substrate surface in response to polishing (Fig. 27), with the quality of the film decreasing for samples further away from the center of the substrate. Films fabricated at $r = 130$ nm show clear evidence of porosity and polishing-induced damage, whereas the film deposited at $r > 130$ nm shows signs of failure and delamination form the surface of the tool. Further examination of the latter coating shows its highly porous morphology, characterized by columns with $d = 200 - 400$ nm. Porosity of the film was quantitatively estimated by comparing the predicted and real dependence of the thickness on the ion current density, assuming linear dependence in the former case.[45] It was found that the coatings fabricated at $J_i \geq 30$–32 A/m^2 had porosity of $<6\%$ and sufficient wear resistance for cutting applications. However, since higher porosity may be desired for such applications as

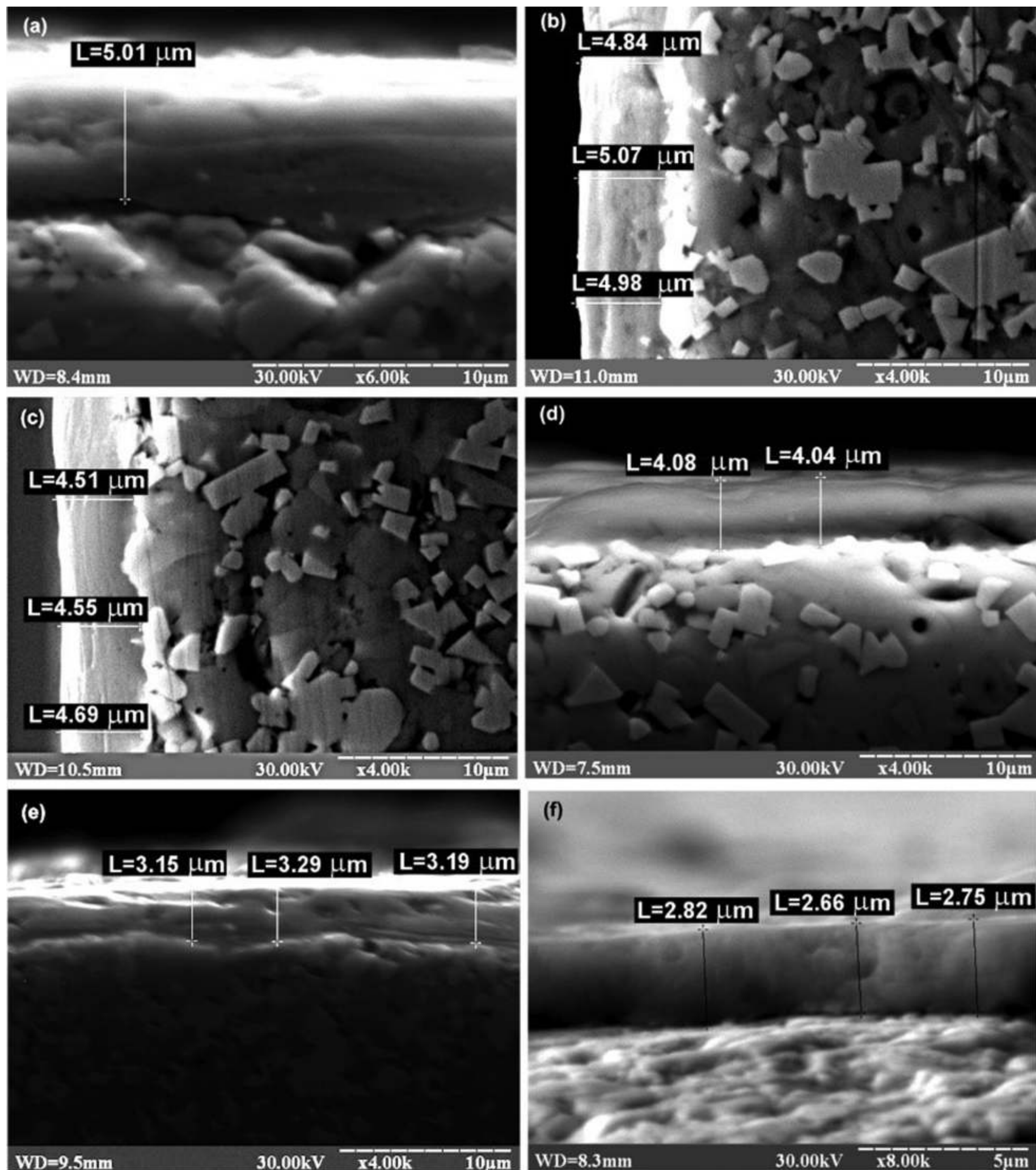

FIG. 27. Representative SEM images of TiN thin films fabricated on the cutting inserts at different points r along the substrate surface, $r = 0$ mm (a); 40 mm (b); 70 mm (c);100 mm (d); 130 mm (e); and 160 mm (f). Thin films in (a)-(d) resist damage by polishing, suggesting improved film density, whereas polishing of film (e) that shows evidence of porosity results in its damage, and an uneven finish. Film (f) experiences significant fracture and peeling as a result of the polishing, suggesting poor mechanical properties. Reprinted with permission from Baranov *et al*., IEEE Trans. Plasma Sci. **41**, 3640 (2013). Copyright 2013 IEEE.

drug delivery or energy storage, the control over the ion current density may provide a useful opportunity for these fields.

Expanding the treatment area to $r \approx 200$ mm with the aim to enhance productivity by 4-fold necessitated the use of the arc magnetic field to enhance the number of ions reaching the surface for ion etching and heating of the substrate in preparation for thin film synthesis [such magnetron mode of operation is illustrated in Fig. 25(c) and Figs. 9(k)–9(m)]. For coating, the magnetic field was modulated into bottle configuration [shown in Figs. 25(d)–25(f)] to uniformly distribute the ion current density across the treatment region, converting it from Gaussian-type[124] to uniform distribution. The respective discharges are shown in Figs. 28(a) and 28(b), respectively. The time-averaged uniform distribution was estimated, with consideration of the rotation of the

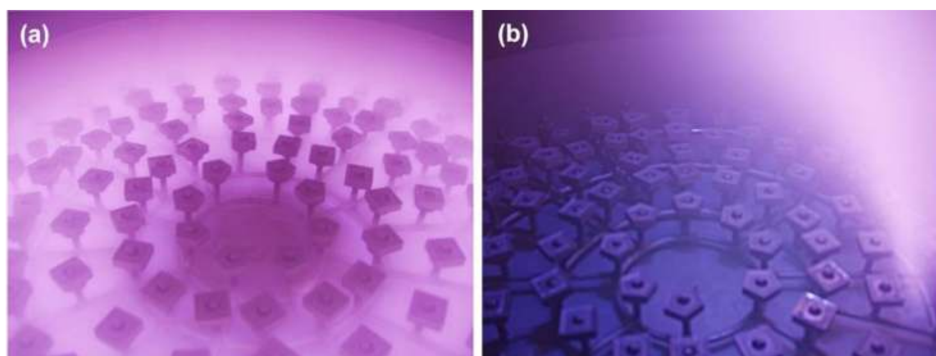

FIG. 28. Images of plasma discharges generated in arc (a) and bottle (b) configuration of the magnetic field, used for sample preparation and deposition of uniform vacuum arc thin films, respectively. De-focused, uniformly distributed ion current is obtained by powering the center under-substrate coil in conjunction with substrate rotation and shifting when operated as a magnetron discharge (a) and by alternative the power between the under-substrate coils in conjunction with substrate rotation when operated as an arc discharge (b). Reprinted with permission from Baranov *et al*., Mater. Chem. Phys. **188**, 143 (2017). Copyright 2017 Elsevier.

substrate with respect to z axis (Fig. 25).[80] While the previous experiments defined the minimum average ion current density of 30–32 A/m^2 for the deposition of wear-resistant TiN coatings,[45] the enhanced configuration used in this experiment delivered an average $J_i \approx 40$ A/m^2 over the substrate, with the enhancement attributed to the effects of the ion flux de-focusing and superposition of the distributions arising from the application of the bottle magnetic fields to the plasma.

In addition to porosity, other important determinants of TiN film wear performance, e.g., morphology, roughness, and crystallinity were explored. Independent of their location on the substrate, all films were found to have a columnar grain structure, with grains elongated perpendicular to the substrate plane, and typically extending through the entire thickness of the film, which is typical for PVD coatings. The grains were densely packed together, with no voids at the crystal boundaries. Interestingly, there was no obvious correlation between the roughness, porosity, and the quality of adhesion of the film and the variations in film thickness for samples fabricated at $r > 160$ mm. For films deposited closer to the center of the substrate, little variation in the mechanical quality of the films was observed, with grain diameter of $\sim$0.2–0.3 μm, and the average surface roughness Ra of <0.13 μm. Samples fabricated within the $r = 110 - 160$ mm region of the substrate had working life 10%–15% longer than that of samples treated closer to the center of the substrate. Coating produced at the $r = 110$ mm point has the highest wear resistance, owing to a favorable combination of low surface roughness $Ra \approx 0.08$ μm and reduced quantity of Ti droplets delivered from the vacuum arc source, which reduces as the workpiece is moved toward the edge of the substrate. The latter effect arises from magnetic field being more efficient at controlling the distribution of plasma than the motion of Ti droplets. As the ion current density decreases, roughness of the films increases for samples treated further away from the substrate center, accounting for the minor reduction in wear resistance. At the same time, the hardness of these deposits increases, from 21 GPa ($r = 30$) to 23 GPa ($r = 160$ mm). At $r = 200$ mm, the highest value of hardness is achieved, at 25 GPa, which provides further evidence for high internal stresses in the film and the *stoichiometric composition* of TiN. The former contributes to poor strength of adhesion between the deposit and the surface of the workpiece.

Overall, magnetically controlling the ion flux makes it possible to increase the processing area by 2.6 times (from $r = 100$ mm to $r = 160$ mm) without sacrificing the performance of the material, within which the use of time-averaged distribution $J_i(r)$ did not notable affect the linear $h(r) = aJ_i(r)$ dependence of the film thickness $h(r)$ on the ion current density.[45] The characteristics of the films fabricated within this zone were improved in comparison to the original deposition, highlighting further opportunities for optimization.

IV. PERSPECTIVES AND TRENDS

Since early experimental setups of 19th century (Fig. 29), plasma-based technologies have undergone tremendous development into highly versatile tools capable of delivery of intricate, highly complex nanostructures and devices in a way that is efficient, economical, and environment- and human-health-friendly.

Early apparatuses were based on the application of DC glow discharge and, hence, unable to control the ion energy and fluxes separately since the relation between these parameters are determined by the current voltage characteristics

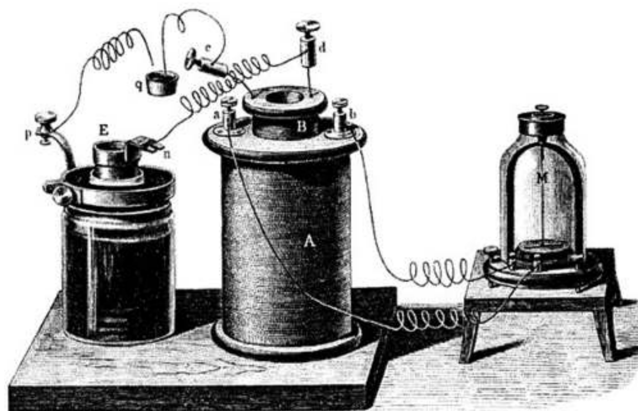

FIG. 29. One of the first experiments on plasma deposition. See detailed description in Ref. 142.

(VAC). Enhanced pressure of the background gas was another limitation of these setups, since it made it difficult to avoid contamination of the processed surface layers. To overcome these limitations, a magnetic field of an arc configuration was introduced above the processed surface (magnetron discharge), thus "splitting" the VAC dependence of the glow discharge by means of the magnetic field.

This facilitated the separation of respective controls over the ion energy and current density to the substrate. In addition, the arc configuration allowed increasing greatly the path of the electrons from the substrate (cathode) to the vacuum chamber walls (anode), thus decreasing the discharge pressure from about 100 to 1 Pa. However, high energy of the ions was still not obtainable for the arc configuration, since arcing occurs at the enhanced DC discharge voltage. In parallel, significant progress was made in our understanding of the processes of magnetic insulation of plasma from the discharge vessel walls in the field of controlled plasma fusion. This knowledge was promptly transferred to technological setups in the form of the magnetic bucket configuration. The resulting configuration with the guiding magnetic field made it possible to control a general flux of the ions from an external plasma source to a substrate.

To obtain the separate control of the ion energy and flux to the substrate, a plasma immersion ion implantation and deposition technique was developed to handle the ion energy within a plasma sheath between the plasma and the biased substrate. Either DC or pulsed bias was applied to the substrate with a purpose of generation of the Child law or matrix sheath to provide the ions with the energy and to prevent the arcing. Development of RF (CCP, ICP) and MW plasma expanded the range of the density of the ion current to the substrate and provided the plasma-enhanced technology with new methods of energy and current density distribution control based on independent powering of the plasma generation and substrate bias circuits. The nominal characteristics of modern plasma setups for vacuum plasma processing and methods of control of ion energy and flux distribution over the substrate are listed in Table I.

As it can be seen, a large variety of plasma sources necessitated the development of an equally wide range of control methods to handle the plasma flux over a substrate. Among them, methods of magnetic control of plasma are the most applied: magnetic traps of arc configurations are used when the substrate is a part of the plasma-generating circuit (ISS), and sets of magnetic mirrors are generated near the plasma source and the substrate to affect the plasma parameters when the substrate is processed with plasma from an external source (ESS).

Let us briefly examine several major tendencies of modern plasma processing technologies. High productivity, low material and energy consumption, implementation of the whole process in a single technological cycle, and uniform processing of large substrates to enhance productivity are among the main efficiency criteria for any technology. In the context of plasma-based technologies for surface processing, high productivity means a sufficiently large surface area treated in a single technological step. The uniform processing of extended substrates is another specific requirement to the plasma-based technology. The low material consumption means the deposition of ion flux to the selected surfaces and prevention of the material loss to the plasma reactor walls. The implementation of the whole process in a single setup allows shortening the processing time by excluding additional processing steps.

✓Thus, what are the major trends?

TABLE I. Nominal characteristics of plasma setups for vacuum plasma processing and methods of control of ion energy and flux distribution to the substrate.

Plasma source	Electron temperature (eV)	Electron density (m^{-3})	Gas pressure (Torr)	Power input (W)	Control of ion flux distribution and energy to the substrate
DC glow discharge	2–5	10^{16}	0.1–5	100–300	Closed drift configuration at the plasma generation region with arc-shaped magnetic field (DC magnetron) (Sec. II C 1 a)
Capacitive coupled plasma	3–8	10^{17}	0.05–1	200–500	Magnetic bucket around the substrate perimeter (RF magnetron, Sec. II C 1 b); control of driving frequency, RF power (dual-frequency CCP etcher) and the substrate shape (Sec. II C 1 c);
Inductively coupled plasma	5–15	10^{18}	10^{-3}–0.1	500–2000	Magnetic bucket around the substrate perimeter (Sec. II C 1 b) or along the vacuum chamber walls (Sec. II C 2 d); Array of ferromagnetic enhanced inductive plasma sources (Sec. II C 2 a); Neutral loop configuration of magnetic field (Sec. II C 2 c)
HiPIMS	1–5	10^{17}–10^{18}	10^{-3}–10^{-2}	200–600	Guiding magnetic field of open drift configuration (Sec. II C 2 e)
Vacuum arc deposition	1–8 eV	10^{17}–10^{18}	10^{-4}–10^{-2}	500–5000	Set of magnetic mirrors under substrate and magnetic mirror at a plasma generation region (Sec. II C 2 i)
Helicon	5–15	10^{18}–10^{19}	0.01–0.1	500–2000	Array of helicon plasma sources (Sec. II C 2 b)
ECR plasma	5–15	10^{18}	10^{-4}–10^{-2}	300–1000	"Resonant" region is determined by magnetic field, thus large uniform plasma can be obtained; a multi-slotted antenna for uniform radiation is used to control the plasma spatial distribution (Sec. II C 2 e)

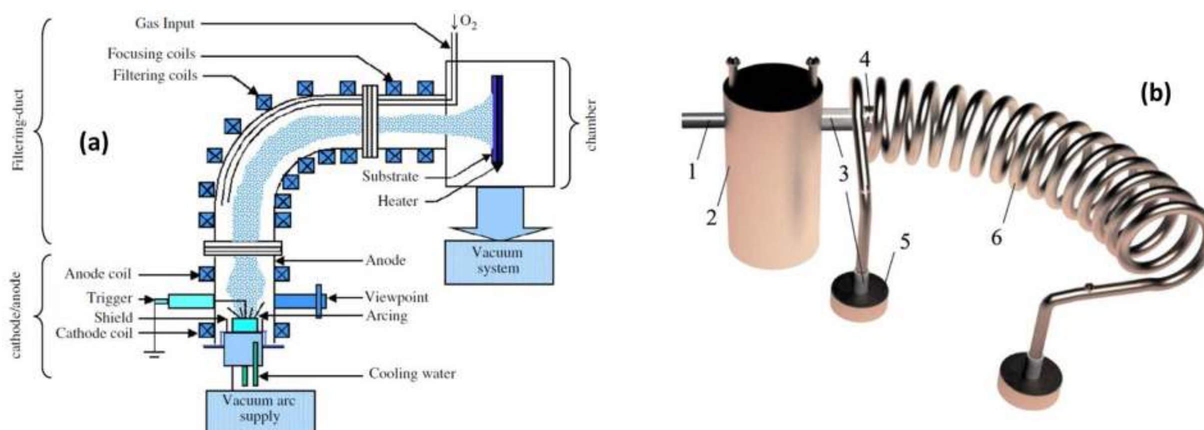

FIG. 30. Vacuum arc plasma source enhanced with macroparticle filter: (a) Conventional design (Reprinted with permission from Yuen *et al*., J. Cryst. Growth 287, 204 (2006). Copyright 2006 Elsevier) and (b) simplified design: 1—cathode, 2—support for plasma source, 3—insulators, 4—first anode, 5— support for macroparticle filter, and 6—macroparticle filter. Reprinted with permission from Rev. Sci. Instrum. **81**, 023506 (2010). Copyright 2010 AIP Publishing LLC.

A. Make it simple

Simplification has distinctive advantages such low cost, reparability, process flexibility associated with rapid reconfigurability of basic plasma setups due to lower nomenclature of parts involved, and replacement of high-skilled personnel by technically qualified persons. The following two schematics can be considered as good examples of such simplification.

Figure 30(a) illustrates a conventional schematic of the FCVA system for the deposition of high-quality ZnO thin films.[143] The system consists of a cathodic vacuum arc source (anode–cathode coils), an off-plane double-bend (OPDB) plasma-filtering duct and a deposition chamber. The filtering duct has two-torus bends at 90° and 45° with respect to axis of the cathodic vacuum arc source. The exterior wall of the filtering duct is surrounded by a set of magnetic coils for the generation of magnetic field to guide the plasma ions. The interior wall of the filtering duct is equipped with baffles that are designed to catch or to reflect macroparticles. A schematic of cathodic filtered vacuum arc plasma source proposed by Chekh *et al.*[144] is an example of a simple design [Fig. 30(b)]: the source without filter has only four components and none of them require precise machining. The source operates in a repetitively pulsed regime, and for laboratory experiments it can be used without water cooling. The system avoids the need for a complicated power supply system for this plasma source, with a single power supply used to ignite the arc, to provide the current for the arc itself, to generate the magnetic field in the filter, and provide its positive electric biasing without any additional high power resistance.

B. Make it sophisticated

There are instances, i.e., deposition of very complex nanosystems and metamaterials,[145] when complex, multistage processes are unavoidable. Hierarchical nanostructures, multicomponent surface alloys, and solid solutions require precise control over phase transitions, crystallinity, doping, carrier density in the photovoltaic materials,[146] morphology control, etc. These demands necessitate plasma reactors with significantly higher level of complexity to facilitate concomitant control over data, energy, and material fluxes. Indeed, for the plasma setup to deliver the desired complexity and quality of the deposit, it should be able to support multiple processing environments, such as by the use of various plasma sources, in-process float and handling systems, complex gas supply system, and data acquisition systems, brought together by a superior design solution, such as that shown in Fig. 31.[69]

C. Make it large

Simplification for large systems may be especially beneficial since the setup productivity shows square law dependence on the substrate diameter, thus a simple 2-fold increase in the diameter results in the fourfold increase in the setup productivity. However, such an increase in the

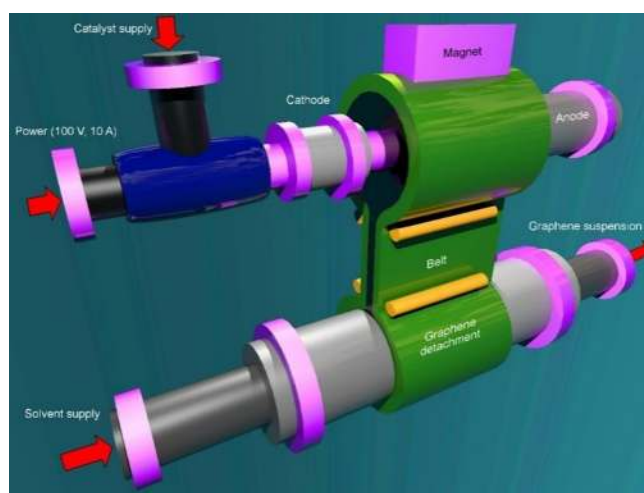

FIG. 31. Concept of the large-scale graphene production system based on arc discharge. The whole apparatus can be sub-divided into several subunits: catalyst, gas, and power supply unit; process unit (chamber, cathode, anode, and magnet); product transportation unit (belt with the necessary guide rolls and actuators), and graphene suspension preparation unit (chamber with solvent washing out the graphene product from the belt and container for the suspension). Reprinted with permission from Levchenko *et al*., Nanoscale **8**, 10511 (2016). Copyright 2016 RSC.

substrate sizes may require sophisticated controls of plasma fluxes extracted from various types of plasma sources. Hence, roll-to-roll in-process of the treated parts can be more beneficial. An example of such a system is presented in Fig. 32, where a schematic of the large-scale equipment for the roll-to-roll microwave plasma chemical vapor deposition process for the production of 294 mm width graphene films at low temperature is shown.[147] However, even in this case, a control of ion fluxes is necessary to shape the flux over the ribbon-like substrate. In this case, for the purpose of uniform large area processing, a system of a magnetically enhanced long-slot microwave plasma source developed by Kuwata and colleagues[148] may be in demand.

D. Make it small

A radically different approach to large-scale synthesis of nanomaterials is based on the use of microplasmas (Fig. 33), the physical properties of which offer distinct advantages over conventional large-volume, reactor-based processing at low pressures.[149] Indeed, such systems allow for the fabrication of a broad range of nanomaterials suspended in gas- and liquid-phase, e.g., aerosol and colloidal nanoparticles, and surface-bound nanostructures, such as hierarchical thin films and nanotube architectures, nanocomposites, to name a few.[150] The flexibility of the processing environment within which microplasma-based systems can operate fueled their rapid development and uptake across a number of fields beyond material synthesis, such as plasma medicine[151] and waste water treatment, giving rise to an impressive range of microplasma-based systems since their emergence in 2002. The simplicity, affordability, and compact design further contributed to their integration into a diverse assortment of processes. Even though the majority of reports in the scientific literature focus on laboratory-scale setups, microplasma-based systems are highly amenable to scale up and integration into existing manufacturing workflows, especially roll-to-roll processing due to the favorable combination of atmospheric-pressure operation and continuous treatment. However, being a relatively new technology, the fundamental understanding of the highly complex reactive environment and physico-chemical processes that take place in these plasmas is still insufficient for large-scale optimization. Indeed, despite some mechanisms that can be inferred from low-pressure plasma systems, the differences in the energy exchange mechanisms that arise from operating at considerably higher pressure should not be ignored. Further complexities arise when modelling and simulating microplasma synthesis processes where chemically reactive gases and liquids, as well as solid metal precursors are employed. It is evident that there is a strong need for a synergistic effort between physicists, chemists, material scientists, and engineers, and the development of appropriate diagnostics tools in order to solve such multidimensional problems and enable further advancement of this family of technologies.[152–154]

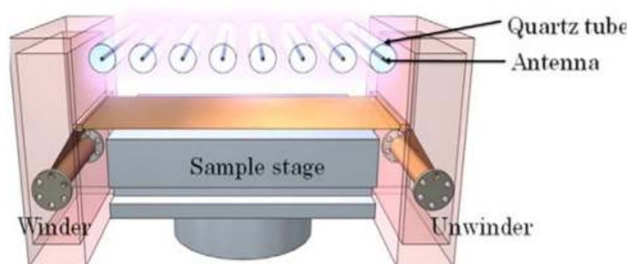

FIG. 32. Schematic of roll-to-roll CVD apparatus for graphene film deposition. Reprinted with permission from Yamada *et al.*, Carbon **50**, 2615 (2012). Copyright 2012 Elsevier.

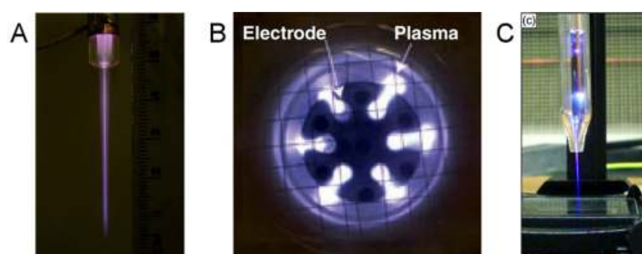

FIG. 33. Examples of moders miniaturized plasma discharges. (a) Typical image of plasma jet for UHV = 3.8 kV, He flow of 15 1/min. Reprinted with permission from Appl. Phys. Lett. **94**, 231504 (2009). Copyright 2009 AIP Publishing LLC. (b) Plasma torch used in the treatment of a chronic infected wound. Reprinted with permission from Isbary *et al.*, Brit. J. Dermatol. **163**, 78 (2010). Copyright 2010, John Wiley and Sons. (c) Atmospheric plasma jet. Reprinted with permission from Fang *et al.*, IEEE Trans. Plasma Sci. **43**, 765 (2015). Copyright 2015, IEEE.

V. CONCLUDING REMARKS

When dealing with the modern plasma processing technology, consolidated effort is needed to further advance this field of immense complexity. Considering a tremendous variety of physical, schematic, construction, and technological solutions of modern plasma-based technological setups for plasma-enabled material processing and other ultramodern applications, the potential user may get lost in the choice. Clear and well-defined physics-based classification and systematization of the entire spectrum of the possible solutions with a clear picture of advantages, key benefits and limitations of each type for any given application, as well as clear decision criteria are necessary to facilitate the choice of the most reliable and cost-effective plasma processing method. This work briefly reviews the plasma processing from the point of view of the most important process, namely, control of plasma fluxes in the most applied types of plasma setups. This control directly determines the delivery of mass and energy to the surfaces subject to the treatment, process uniformity, energy spectra of plasma ions, as well as key parameters such as growth and modification rates, intensity of energy input determining phase transitions, crystallinity, generation of lattice defects, doping, metastructure formation, and other key parameters. The work will be useful for the physicists working in the field of technological plasma and material processing, as well as setup designers to give them a comprehensive view and understanding of the key physical processes. It also benefits end users to facilitate orientation in a wide spectrum of this kind of ultramodern physics-based equipment and ensure correct selection of the specific process and equipment for the particular application niche.

ACKNOWLEDGMENTS

This work was supported by the Grant No. 11405038, 1894 EDB (OSTIn), National Research Foundation, Singapore, and Academic Research Fund AcRF Tier1 RP6/16. I.L. acknowledges the support from the School of Chemistry, Physics and Mechanical Engineering, Science and Engineering Faculty, Queensland University of Technology. U.C. would like to acknowledge support of Slovenian Research Agency (ARRS) (Grant nos. L2-7667 and L2-7499).

[1]M. A. Lieberman and A. J. Lichtenberg, *Principles of Plasma Discharges for Materials Processing* (Wiley Interscience, New York, 2005).
[2]S. Walia, C. M. Shah, P. Gutruf, H. Nili, D. R. Chowdhury, W. Withayachumnankul, M. Bhaskaran, and S. Sriram, Appl. Phys. Rev. **2**, 011303 (2015).
[3]A. Anders, *Handbook of Plasma Immersion Ion Implantation and Deposition* (John Wiley & Sons, New York, 2000).
[4]Z. Li and F. Chen, Appl. Phys. Rev. **4**, 011103 (2017).
[5]M. M. M. Bilek, D. V. Bax, A. Kondyurin, Y. Yin, N. J. Nosworthy, K. Fisher, A. Waterhouse, A. S. Weiss, C. G. dos Remedios, and D. R. McKenzie, Proc. Natl. Acad. Sci. U. S. A. **108**, 14405 (2011).
[6]M. V. Jacob, K. Bazaka, D. Taguchi, T. Manaka, and M. Iwamoto, Chem. Phys. Lett. **528**, 26 (2012).
[7]L. Bruchhaus, P. Mazarov, L. Bischoff, J. Gierak, A. D. Wieck, and H. Hövel, Appl. Phys. Rev. **4**, 011302 (2017).
[8]I. Levchenko, K. Ostrikov, K. Diwan, K. Winkler, and D. Mariotti, Appl. Phys. Lett. **93**, 183102 (2008).
[9]A. Dey, A. Chroneos, N. S. J. Braithwaite, R. P. Gandhiraman, and S. Krishnamurthy, Appl. Phys. Rev. **3**, 021301 (2016).
[10]K. Bazaka, M. V. Jacob, and K. Ostrikov, Chem. Rev. **116**, 163 (2016).
[11]V.-S. Dang, H. Parala, J. H. Kim, K. Xu, N. B. Srinivasan, E. Edengeiser, M. Havenith, A. D. Wieck, T. de los Arcos, R. A. Fischer, and A. Devi, Phys. Status Solidi A **211**(2), 416 (2014).
[12]J. Ahmad, K. Bazaka, and M. V. Jacob, Electronics **3**, 266 (2014).
[13]G. Scheunert, O. Heinonen, R. Hardeman, A. Lapicki, M. Gubbins, and R. M. Bowman, Appl. Phys. Rev. **3**, 011301 (2016).
[14]K.-W. Weng, S. Han, Y.-C. Chen, and D.-Y. Wang, J. Mater. Process. Technol. **203**, 117 (2008).
[15]I.-W. Park and K. H. Kim, J. Mater. Process. Technol. **130–131**, 254 (2002).
[16]M. Keidar, A. Shashurin, O. Volotskova, M. A. Stepp, P. Srinivasan, A. Sandler, and B. Trink, Phys. Plasmas **20**, 057101 (2013).
[17]X. Lu, Z. Xiong, F. Zhao, Y. Xian, Q. Xiong, W. Gong, C. Zou, Z. Jiang, and Y. Pan, Appl. Phys. Lett. **95**, 181501 (2009).
[18]F. F. Chen and J. P. Chang, *Lecture Notes on Principles of Plasma Processing* (Plenum/Kluwer Publishers, New York, 2002).
[19]S. Zeb, M. Sadiq, A. Qayyum, G. Murtaza, and M. Zakaullah, Mater. Chem. Phys. **103**, 235 (2007).
[20]I. Levchenko, M. Keidar, S. Xu, H. Kersten, and K. Ostrikov, J. Vac. Sci. Technol. B **31**, 050801 (2013).
[21]J. Bohlmark, M. Östbye, M. Lattemann, H. Ljungcrantz, T. Rosell, and U. Helmersson, Thin Solid Films **515**, 1928 (2006).
[22]A. Anders, J. Andersson, and A. Ehiasarian, J. Appl. Phys. **102**, 113303 (2007).
[23]D. Magnfält, E. Melander, R. D. Boyd, V. Kapaklis, and K. Sarakinos, J. Appl. Phys. **121**, 171918 (2017).
[24]J. Houska, J. Vlcek, S. Potocky, and V. Perina, Diamond Relat. Mater. **16**, 29 (2007).
[25]S. B. Jin, Y. S. Choi, Y. J. Kim, I. S. Choi, and J. G. Han, Surf. Coat. Technol. **205**, S139 (2010).
[26]A. Anders, IEEE Trans. Plasma Sci. **30**, 108 (2002).
[27]J. H. Huang, C. H. Lin, C. H. Ma, and H. Chen, Scr. Mater. **42**, 573 (2000).
[28]S. Guruvenket and G. M. Rao, J. Vac. Sci. Technol. A **20**(3), 678 (2002).
[29]A. Michelmore, D. A. Steele, D. E. Robinson, J. D. Whittle, and R. D. Short, Soft Matter. **9**, 6167 (2013).
[30]C.-S. Shin, D. Gall, Y.-W. Kim, N. Hellgren, I. Petrov, and J. E. Greene, J. Appl. Phys **92**(9), 5084 (2002).
[31]S. Kumar, I. Levchenko, K. Ostrikov, and J. A. McLaughlin, Carbon **50**, 325 (2012).
[32]C. Chen and C. Liu, J. Electron. Mater. **34**(11), 1408 (2005).
[33]I. Levchenko, M. Romanov, M. Keidar, and I. I. Beilis, Appl. Phys. Lett. **85**, 2202–2204 (2004).
[34]Q. Cheng and S. Xu, J. Phys. Chem. C **113**, 14759 (2009).
[35]D. H. C. Chua, K. B. K. Teo, T. H. Tsai, W. I. Milne, D. Sheeja, B. K. Tay, and D. Schneider, Appl. Surf. Sci. **221**, 455 (2004).
[36]D. Li, W. Xie, and C. I. Zou, Appl. Phys. A **122**, 307 (2016).
[37]U. Sharma, S. S. Chauhan, J. Sharma, A. K. Sanyasi, J. Ghosh, K. K. Choudhary, and S. K. Ghosh, J. Phys.: Conf. Ser. **755**, 012010 (2016).
[38]T. Kubarta and A. Aijaz, J. Appl. Phys. **121**, 171903 (2017).
[39]S. Schmidt, T. Hänninen, J. Wissting, L. Hultman, N. Goebbels, A. Santana, M. Tobler, and H. Högberg, J. Appl. Phys. **121**, 171904 (2017).
[40]K. G. F. Janssens, D. Olmsted, E. A. Holm, S. M. Foiles, S. J. Plimpton, and P. M. Derlet, Nature Mater. **5**, 124 (2006).
[41]I. Levchenko, K. Ostrikov, and A. B. Murphy, J. Phys. D: Appl. Phys. **41**, 092001 (2008).
[42]A. Anders, Thin Solid Films **518**, 4087 (2010).
[43]I. Petrov, P. B. Barna, L. Hultman, and J. E. Greene, J. Vac. Sci. Technol. A **21**(5), 117 (2003).
[44]G. Filipič, O. Baranov, M. Mozetič, K. Ostrikov, and U. Cvelbar, Phys. Plasmas **21**, 113506 (2014).
[45]O. Baranov, J. Fang, A. Rider, S. Kumar, and K. Ostrikov, IEEE Trans. Plasma Sci. **41**(12), 3640 (2013).
[46]N. S. J. Braithwaite, Plasma Sources Sci. Technol **9**(4), 517 (2000).
[47]A. Fridman and L. A. Kennedy, *Plasma Physics and Engineering* (CRC Press, Taylor & Francis Group, New York, 2004).
[48]V. Brackmann, V. Hoffmann, A. Kauffmann, A. Helth, J. Thomas, H. Wendrock, J. Freudenberger, T. Gemming, and J. Eckert, Mater. Charact. **91**, 76 (2014).
[49]W. Jiang, J. Tang, Y. Wang, W. Zhao, and Y. Duan, Sci. Rep. **4**, 6323 (2014).
[50]C. C. Farnell, J. D. Williams, and C. C. Farnell, Plasma Sources Sci. Technol. **20**, 025006 (2011).
[51]P. Saikia, B. K. Saikia, K. S. Goswami, and A. Phukan, J. Vac. Sci. Technol. A **32**, 031303 (2014).
[52]A. Anders, Surf. Coat. Technol. **205**, S1 (2011).
[53]J. T. Gudmundsson, Plasma Phys. Controlled Fusion **58**, 014002 (2015).
[54]A. Anders, J. Appl. Phys. **121**, 171101 (2017).
[55]D. Grondona, H. Kelly, and F. O. Minotti, J. Appl. Phys. **99**, 043304 (2006).
[56]R. K. Amirov, N. A. Vorona, A. V. Gavrikov, G. D. Liziakin, V. P. Polistchook, I. S. Samoylov, V. P. Smirnov, R. A. Usmanov, and I. M. Yartsev, IOP Conf. Ser.: J. Phys. Conf. Ser. **830**, 012059 (2017).
[57]L. L. Alves, L. Marques, C. D. Pintassilgo, G. Wattieaux, E. Es-sebbar, J. Berndt, E. Kovacević, N. Carrasco, L. Boufendi, and G. Cernogora, Plasma Sources Sci. Technol. **21**, 045008 (2012).
[58]G. Primc, I. Levchenko, S. Kumar, U. Cvelbar, M. Mozetic, and K. Ostrikov, IEEE Trans. Plasma Sci. **42**, 2564 (2014).
[59]A. Sun, M. M. Becker, and D. Loffhagen, Comput. Phys. Commun. **206**, 35 (2016).
[60]Y. Liu, Ch. Ye, H. He, X. Wang, S. Ge, and F. Huang, Thin Solid Films **579**, 1 (2015).
[61]Y. Jeong, Y. J. Lee, D.-C. Kwon, and H. Choe, Curr. Appl. Phys. **17**, 403 (2017).
[62]F. F. Chen and H. Torreblanca, IEEE Trans. Plasma Sci. **39**, 2452 (2011).
[63]I. A. Kotelnikov, Phys. Plasmas **21**, 122101 (2014).
[64]M. Kaiser, K.-M. Baumgartner, and A. Mattheus, Contrib. Plasma Phys. **52**, 629 (2012).
[65]A. Metel, Surf. Coat. Technol. **156**, 38 (2002).
[66]A. W. Chao, K. H. Mess, M. Tigner, and F. Zimmermann, *Handbook of Accelerator Physics and Engineering* (World Scientific Publishing Co. Pte. Ltd., 2013).
[67]M. C. Salvadori, F. S. Teixeira, L. G. Sgubin, W. W. R. Araujo, R. E. Spirin, E. M. Oks, K. M. Yu, and I. G. Brown, Appl. Phys. Lett. **101**, 224104 (2012).
[68]S. C. Gallo, A. E. Crespi, F. Cemin, C. A. Figueroa, and I. J. R. Baumvol, IEEE Trans. Plasma Sci. **39**(11), 3028 (2011).
[69]I. Levchenko, K. Ostrikov, J. Zheng, X. Li, M. Keidar, and K. Teo, Nanoscale **8**, 10511 (2016).
[70]U. Vogel, C. Klaus, C. Nobis, and J. W. Bartha, Thin Solid Films **520**(20), 6404 (2012).
[71]O. Baranov, J. Fang, M. Keidar, X. Lu, U. Cvelbar, and K. Ostrikov, IEEE Trans. Plasma Sci. **42**(10), 2464 (2014).
[72]R. De Gryse, J. Haemers, W. P. Leroy, and D. Depla, Thin Solid Films **520**(18), 5833 (2012).

[73]L. Wen, M. Kumar, B. B. Sahu, S. B. Jin, C. Sawangrat, K. Leksakul, and J. G. Han, Surf. Coat. Technol. **284**, 85 (2015).
[74]O. Baranov, X. Zhong, J. Fang, S. Kumar, S. Xu, U. Cvelbar, D. Mariotti, and K. Ostrikov, IEEE Trans. Plasma Sci. **42**(10), 2518 (2014).
[75]I. Levchenko, M. Romanov, and M. Keidar, J. Appl. Phys **94**(3), 1408 (2003).
[76]J. Lu, G. Tao, C. G. Lee, J. H. Yoon, and T. Y. Cho, Vacuum **85**(6), 657 (2011).
[77]D. Hagedorn, F. Löffler, and R. Meeß, Surf. Coat. Technol. **203**, 632 (2008).
[78]I. Levchenko, M. Romanov, O. Baranov, and M. Keidar, Vacuum **72**, 335 (2004).
[79]A. Bogaerts, E. Bultinck, I. Kolev, L. Schwaederl, K. Van Aeken, G. Buyle, and D. Depla, J. Phys. D: Appl. Phys. **42**, 194018 (2009).
[80]O. Baranov, J. Fang, K. Ostrikov, and U. Cvelbar, Mater. Chem. Phys. **188**, 143 (2017).
[81]J. Musil, P. Baroch, J. Vlček, K. H. Nam, and J. G. Han, Thin Solid Films **475**(1-2), 208 (2005).
[82]V. Linss, Surf. Coat. Technol. **241**, 19 (2014).
[83]O. Baranov, M. Romanov, M. Wolter, S. Kumar, X. Zhong, and K. Ostrikov, Phys. Plasmas **17**, 053509 (2010).
[84]K. Honglertkongsakul, S. Chaiyakun, N. Witit-anun, W. Kongsri, and P. Limsuwan, Procedia Eng. **32**, 962 (2012).
[85]I. V. Svadkovski, D. A. Golosov, and S. M. Zavatskiy, Vacuum **68**, 283 (2003).
[86]O. Baranov, M. Romanov, S. Kumar, X. Zhong, and K. Ostrikov, J. Appl. Phys. **109**(6), 063304 (2011).
[87]G. Brauer, B. Szyszka, M. Veröhl, and R. Bandorf, Vacuum **84**, 1354 (2010).
[88]P. J. Kelly and R. D. Arnell, Vacuum **56**, 159 (2000).
[89]D. M. Mattox, *Handbook of Physical Vapor Deposition (PVD) Processing* (Cambridge University Press, 2014).
[90]S. M. Rossnagel, J. Vac. Sci. Technol. A **21**(5), S74 (2003).
[91]D. W. Kim, H. Y. Lee, S. J. Kyoung, H. S. Kim, Y. J. Sung, S. H. Chae, and G. Y. Yeom, IEEE Trans. Plasma Sci. **32**(3), 1362 (2004).
[92]M. J. Kushner, J. Appl. Phys. **94**(3), 1436 (2003).
[93]M. A. Lieberman, J. P. Booth, P. Chabert, J. M. Rax, and M. M. Turner, Plasma Sources Sci. Technol. **11**, 283 (2002).
[94]D. Sung, V. Volynets, W. Hwang, Y. Sung, S. Lee, M. Choi, and G.-H. Kim, J. Vac. Sci. Technol. A **30**(6), 061301 (2012).
[95]A. Perret, P. Chabert, J.-P. Booth, J. Jolly, J. Guillon, and Ph. Auvray, Appl. Phys. Lett. **83**(2), 243 (2003).
[96]A. Perret, P. Chabert, J. Jolly, and J.-P. Booth, Appl. Phys. Lett. **86**, 021501 (2005).
[97]V. Volynets, H. Shin, D. Kang, and D. Sung, J. Phys. D: Appl. Phys. **43**, 085203 (2010).
[98]V. N. Volynets, A. G. Ushakov, D. Sung, Y. N. Tolmachev, V. G. Pashkovsky, J. B. Lee, T. Y. Kwon, and K. S. Jeong, J. Vac. Sci. Technol. A **26**(3), 406 (2008).
[99]T. Meziani, P. Colpoand, and F. Rossi, Plasma Sources Sci. Technol. **10**, 276 (2001).
[100]V. Godyak, J. Phys. D: Appl. Phys. **46**, 283001 (2013).
[101]F. F. Chen, Plasma Sources Sci. Technol. **24**, 014001 (2015).
[102]F. F. Chen and H. Torreblanca, Phys. Plasmas **16**, 057102 (2009).
[103]T. Uchida and S. Hamaguchi, J. Phys. D: Appl. Phys. **41**, 083001 (2008).
[104]Y. Sakurai and T. Osaga, IEEE Trans. Plasma Sci. **39**(11), 2550 (2011).
[105]Y. Asami and H. Sugawara, IEEE Trans. Plasma Sci. **42**(10), 2540 (2014).
[106]F. Chen, *Introduction to Plasma Physics and Controlled Fusion* (Plenum, New York, 1984).
[107]D. Tang and P. K. Chu, Appl. Phys. Lett. **82**, 2014 (2003).
[108]Y. Yasaka, K. Koga, N. Ishii, T. Yamamoto, M. Ando, and M. Takahashi, Phys. Plasmas **9**(3), 1029–1035 (2002).
[109]Y. Yasaka, N. Ishii, T. Yamamoto, M. Ando, and M. Takahashi, IEEE Trans. Plasma Sci. **32**(1), 101 (2004).
[110]Y. Yasaka, N. Tobita, and A. Tsuji, AIP Adv. **3**, 122102 (2013).
[111]J. H. Bowles, D. Duncan, D. N. Walker, W. E. Amatucci, and J. A. Antoniades, Rev. Sci. Instrum. **67**(2), 455 (1996).
[112]F. Fietzke, H. Morgner, and S. Gunther, Plasma Process. Polym. **6**, S242–S246 (2009).
[113]A. Anders and J. Brown, IEEE Trans. Plasma Sci. **39**(11), 2528 (2011).
[114]A. Anders, *Cathodic Arcs: From Fractal Spots to Energetic Condensation* (Springer, New York, 2008).
[115]I. I. Aksenov, D. S. Aksyonov, V. V. Vasilyev, A. A. Luchaninov, E. N. Reshetnyak, and V. E. Strelnitskij, IEEE Trans. Plasma Sci. **37**, 1511 (2009).
[116]M. M. M. Bilek, A. Anders, and I. G. Brown, Plasma Sources Sci. Technol. **10**, 606 (2001).
[117]J. Musil, RSC Adv. **5**, 60482–60495 (2015).
[118]I. Levchenko, M. Romanov, and M. Korobov, "Plasma jet interaction with a spherical target in magnetic field," IEEE Trans. Plasma Sci. **32**, 2139 (2004).
[119]A. A. Lisenkov, I. V. Burov, and V. A. Pavlova, Plasma Devices Oper. **10**, 9 (2002).
[120]I. Levchenko and O. Baranov, Vacuum **72**, 205 (2003).
[121]O. Baranov and M. Romanov, Plasma Process. Polym **6**(2), 95 (2009).
[122]O. Baranov, M. Romanov, J. Fang, U. Cvelbar, and K. Ostrikov, J. Appl. Phys **112**(7), 073302 (2012).
[123]V. L. Paperny, V. I. Krasov, N. V. Astrakchantsev, and N. V. Lebedev, J. Phys.: Conf. Ser. **552**, 012007 (2014).
[124]O. Baranov and M. Romanov, Plasma Process. Polym. **5**, 256 (2008).
[125]A. Vesel and M. Mozetič, Vacuum **80**, 253 (2005).
[126]A. I. Morozov and V. V. Savelyev, in *Review of Plasma Physics*, edited by B. B. Kadomtsev and V. D. Shafranov (Consultant Bureau, New York, 2000), Vol. 21, p. 203.
[127]L. D. Landau and E. M. Lifshitz, *Mechanics* (Butterworth-Heinemann, Oxford, 1976).
[128]N. Gyergyek and J. Kovačič, Phys. Plasmas **22**, 043502 (2015).
[129]T. K. Popov, M. Dimitrova, P. Ivanova, J. Kovačič, T. Gyergyek, R. Dejarnac, J. Stockel, M. A. Pedrosa, D. Lopez-Bruna, and C. Hidalgo, Plasma Sources Sci. Technol. **25**, 033001 (2016).
[130]S. Costea, B. Fonda, J. Kovačič, T. Gyergyek, B. S. Schneider, R. Schrittwieser, and C. Ionita, Rev. Sci. Instrum. **87**, 053510 (2016).
[131]M. G. Kong, B. N. Ganguly, and R. F. Hicks, Plasma Sources Sci. Technol. **21**(3), 030201 (2012).
[132]X. P. Lu, Z. H. Jiang, Q. Xiong, Z. Y. Tang, and Y. Pan, Appl. Phys. Lett. **92**(15), 151504 (2008).
[133]I. Denysenko and N. A. Azarenkov, J. Phys. D: Appl. Phys. **44**(17), 174031 (2011).
[134]L. M. Yang, A. K. Tieu, D. P. Dunne, S. W. Huang, H. J. Li, D. Wexler, and Z. Y. Jiang, Wear **267**(5), 233 (2009).
[135]W. Zhou, X. X. Zhong, X. C. Wu, L. Q. Yuan, Q. W. Shu, W. Li, and Y. X. Xia, J. Phys. D: Appl. Phys. **40**(1), 219 (2007).
[136]I. Levchenko, M. Korobov, M. Romanov, and M. Keidar, J. Phys. D: Appl. Phys. **37**(12), 1690 (2004).
[137]Q. Cheng, S. Xu, and S. Huang, IEEE Trans. Plasma Sci. **36**(4), 870 (2008).
[138]D. Manova, J. W. Gerlach, and S. Mandl, Materials **3**(8), 4109 (2010).
[139]K. Ostrikov, S. Kumar, Q. J. Cheng, A. E. Rider, M. M. A. Yajadda, Z. J. Han, D. H. Seo *et al.*, IEEE Trans. Plasma Sci. **39**, 2796 (2011).
[140]H. Fager, O. Tengstrand, J. Lu, S. Bolz, B. Mesic, W. Kölker, Ch. Schiffers, O. Lemmer, J. E. Greene, L. Hultman, I. Petrov, and G. Greczynski, J. Appl. Phys. **121**, 171902 (2017).
[141]E. Isakov, *Cutting Data for Turning of Steel* (Industrial Press, Inc., 2009).
[142]A. Anders, Surf. Coat. Technol. **156**, 3 (2002).
[143]C. Yuen, S. F. Yu, S. P. Lau, and G. C. K. Chen, J. Cryst. Growth **287**, 204 (2006).
[144]Y. Chekh, I. S. Zhirkov, and M. P. Delplancke-Ogletree, Rev. Sci. Instrum. **81**, 023506 (2010).
[145]I. Levchenko, K. Bazaka, M. Keidar, S. Xu, and J. Fang, "Hierarchical Multi-Component Inorganic Metamaterials: Intrinsically Driven Self-Assembly at Nanoscale," Adv. Mater. (published online).
[146]P. W. Sutter, P. M. Albrecht, and E. A. Sutter, Appl. Phys. Lett. **97**, 213101 (2010).
[147]T. Yamada, M. Ishihara, J. Kim, M. Hasegawa, and S. Iijima, Carbon **50**, 2615 (2012).
[148]Y. Kuwata, T. Kasuya, N. Miyamoto, and M. Wada, Rev. Sci. Instrum. **87**, 02C104 (2016).
[149]A. Shashurin, M. N. Shneider, A. Dogariu, R. B. Miles, and M. Keidar, Appl. Phys. Lett. **96**, 171502 (2010).
[150]K. H. Schoenbach and K. Becker, Eur. Phys. J. D **70**, 29 (2016).
[151]G. Isbary, G. Morfill, H. U. Schmidt, M. Georgi, K. Ramrath, J. Heinlin, S. Karrer, M. Landthaler, T. Shimizu, B. Steffes, W. Bunk, R. Monetti, J. L. Zimmermann, R. Pompl, and W. Stolz, Brit, J. Dermatol. **163**, 78 (2010).
[152]D. Mariotti and R. M. Sankaran, J. Phys. D: Appl. Phys. **43**, 323001 (2010).
[153]L. Lin and Q. Wang, Plasma Chem. Plasma Proc. **35**, 925 (2015).
[154]A. C. Ferrari, F. Bonaccorso, V. Fal'ko, K. S. Novoselov *et. al.*, Nanoscale **7**, 4598 (2015).